Issue 21, 2017

Previous Article | Next Article

From the journal:
Dalton Transactions

Sequential incorporation of metallic cations (Cd^{2+} and Hg^{2+}) and *N*-octylamine into titanium phosphate nanoparticles and their subsequent release in acid media

Javier Carrasco-Rodríguez,[a] Daniel Martín-Yerga,[b] Leoncio Garrido,[c] Agustín Costa-García[b] and Francisco J. García Alonso*[a]

Author affiliations

* Corresponding authors

[a] Nanobioanalysis Group, Department of Inorganic and Organic Chemistry, University of Oviedo, 33006, Oviedo, Spain
E-mail: fjga@uniovi.es
Tel: +34 985103525

[b] Nanobioanalysis Group, Department of Physical and Analytical Chemistry, University of Oviedo, 33006, Oviedo, Spain

[c] Departamento de Química Física, Instituto de Ciencia y Tecnología de Polímeros, ICTP-CSIC, Juan de la Cierva 3, 28006 Madrid, Spain

Sequential incorporation of metallic cations (Cd^{2+} and Hg^{2+}) and N-Octylamine into Titanium Phosphate Nanoparticles and their subsequent release in acid media

Javier Carrasco-Rodríguez[a], *Daniel Martín-Yerga*[b], *Leoncio Garrido*[c], *Agustín Costa-García*[b], *Francisco J. García Alonso**[a].

a) Nanobioanalysis group, Department of Inorganic and Organic Chemistry, University of Oviedo, 33006, Oviedo (Spain)

b) Nanobioanalysis Group, Department of Physical and Analytical Chemistry, University of Oviedo, 33006, Oviedo (Spain)

c) Departamento de Química Física, Instituto de Ciencia y Tecnología de Polímeros, ICTP-CSIC, Juan de la Cierva 3, 28006 Madrid, Spain

* Corresponding author: Francisco J. García Alonso

Departament of Inorganic and Oganic Chemistry

University of Oviedo

Julián Clavería 8, 33006, Oviedo (Spain)

E-mail: fjga@uniovi.es

Telephone: (+34) 985103525

ABSTRACT

Titanium Phosphate nanoparticles, TPNP, consisting of a $NaTi_2(PO_4)_3$ core and a shell of hydrogenphosphate and dihydrogenphosphate of Titanium, undergo fast hydrolysis in water releasing phosphoric acid. This reaction is inhibited in the presence of metallic ions like Cd^{2+} or Hg^{2+}, which are able to replace the protons of the shell acid phosphates. The amount of the adsorbed metallic cations could be regulated using counterions of different basicity. The resulting nanoparticles also incorporate $NH_2(CH_2)_7CH_3$ (N-octylamine) at room temperature forming N-octylammonium/phosphate ion pairs, but it was found that at higher cation concentration inside the nanoparticle, a lower amount of amine was adsorbed. The metallic cations and N-octylamine are released in acid media, but the starting material is not fully recovered.

INTRODUCTION

The transition metal phosphates constitute an active field of investigation both in academy and industry.[1,2] Among them, titanium phosphates have found applications mainly as ionic exchangers[3–9] and catalysts,[10–15] although they have also been used for other purposes like ionic conductors,[16] molecular sorbents,[17] semiconductors and photocatalysts.[18] Titanium phosphates present a great variety of structures, from the well-known layered species[19–22] to amorphous materials,[23] including, inter alia, films,[6] fibers,[24] nanoparticles,[25,26,14] hollow nanospheres,[9] and nanotubes.[27]

Titanium phosphate nanoparticles, hereafter named TPNP, obtained using docusate sodium salt (DOSS), orthophosphoric acid (85%) and titanium(IV) n-butoxide as the starting materials are particularly interesting.[25] They possess a core of crystalline $NaTi_2(PO_4)_3$ and a shell of amorphous hydrogenphosphate and dihydrogenphosphate of titanium. Similar titanium phosphate nanoparticles using sodium dodecyl sulfate instead of sodium docusate (DOSS) as surfactant have been prepared.[26]

The sodium dititanium triphosphate, $NaTi_2(PO_4)_3$, is able to insert lithium[28] and extra sodium ions[29,30] and to exchange Na^+ by Ag^+ cations[31] and protons.[32] Furthermore, the $NaTi_2(PO_4)_3$ crystals are luminescent,[33] they show a band emission around 750 nm, probably due to Ti^{3+} impurities, which is very sensible to the titanium environment, particularly to the insertion of foreign ions and the crystallinity of the sample.

On the other hand, TPNP can act as Brønsted acid catalysts[25] and as ion exchangers[34] because of the presence of acid phosphates in the shell. In fact, the TPNP are able to catalyze the ketalization of cyclohexanone and 1,2-ethanediol to cyclohexanone ethylene ketal.[25] They can also be loaded with zinc(II)[34] and cadmium (II)[35,36,34] cations and, after being functionalized with a predetermined protein, they can be used as signal tags for electrochemical biosensors.

The ion-exchange properties of the titanium phosphates have been studied in some detail in the case of the amorphous $Ti(HPO_4)_2$.[7] Thus, it has been found that $Ti(HPO_4)_2$ exhibits higher affinity

57 towards Pb^{2+} over Zn^{2+} and Cd^{2+}, even in the presence of Ca^{2+} at different concentrations. This result
58 is not anticipated when the Hard and Soft Acid and Bases (HSAB) principle is applied, since Ca^{2+} is
59 harder than Pb^{2+}. Nevertheless, it fits well with the log Ksp (Solubility Product Constant) values of
60 the metal phosphates. On the other hand, it has been established that only half of the exchangeable
61 hydrogen ion in amorphous Titanium phosphate is accessible for Pb^{2+} exchange under neutral or
62 acidic solution pH, and the rest is available only for the alkaline solution.

63 Our group is also interested in this kind of nanoparticles[37,38] and we considered that some
64 additional insight could assist to understand better the ion exchange process, as well as the
65 subsequent addition of proteins, two of the main points in preparing labels for the fabrication of
66 electrochemical biosensors. In this paper, we present the first results of our study, using cadmium (II)
67 and mercury(II) as interchangeable cations with TPNP and N-octylamine as a model for the more
68 complicated proteins.

69

70 **EXPERIMENTAL SECTION**

71 **Materials and Reagents**

72 Titanium (IV) butoxide, docusate sodium salt (DOSS), crystalline H_3PO_4 (≥99.999%),
73 cadmium (II) nitrate tetrahydrate, cadmium (II) acetate dihydrate, cadmium (II) acetylacetonate
74 mercury(II) nitrate monohydrate, mercury(II) acetate were purchased from Sigma-Aldrich and used
75 as received. Absolute ethanol and diethyl ether were purchased from VWR and used without further
76 purification. Ultrapure water was obtained with a Millipore Direct Q5 purification system from
77 Millipore Ibérica S. A. (Madrid, Spain).

78

79 **Instrumentation**

80 The high-resolution transmission electron micrographs (HRTEM) were obtained on a JEOL
81 JEM 2100 transmission electron microscope with an accelerating voltage of 200 kV. X-ray

diffraction (XRD) patterns were performed with a Bruker D8 X-ray diffractometer with a Cu Kα X-ray source, λ= 0.15418 nm. Fourier transform infrared (FTIR) spectroscopic measurements were measured on a Perkin Elmer FT Paragon 1000 using KBr pressed disks.

The ^{31}P solid state NMR measurements were performed on a Bruker Avance 400 spectrometer equipped with a 89 mm wide bore, 9.4 T superconducting magnet (^{31}P Larmor frequency at 161.98 MHz). Samples of TPNP were placed in 4 mm zirconia rotor. All reported data were acquired at room temperature. A standard Bruker double resonance 4 mm cross-polarization (CP)/magic angle spinning (MAS) NMR probe head was used. The ^{31}P MAS spectra were acquired using a single pulse excitation (4.15 μs) with high power proton decoupling. A 10 s recycle delay and a MAS spinning rate of 10 kHz were used. The number of acquired scans was 164. A CP pulse sequence with varying contact time and followed by high-power proton decoupling was used to acquire de ^{31}P CP/MAS spectra of TPNPs, at a MAS rate of 6 kHz. In all cases, the free-induction decays were subjected to standard Fourier transformation with 20 Hz line broadening and phasing. The chemical shifts were externally referenced to phosphoric acid 85% (0.0 ppm).

Fluorescence spectra were recorded on a "Varian Carey Eclipse" Luminescence Spectrophotometer using a fixed excitation wavelength of 265 nm with both excitation and emission slit width of 10 nm. The measurements of absorbance and fluuorescence were carried out using conventional Quartz SUPRASIL cuvettes (Hellma Analytics, Germany).

Voltammetric determination of metals

The quantification of metals in the solutions of the synthesis and after the acid treatment was carried out by a voltammetric method. Screen-printed carbon electrodes (DRP-110, DropSens) were used to perform the measurements using a μStat8000 potentiostat (DropSens). Square-wave anodic stripping voltammetry was used as the electrochemical technique due to its good performance for metallic quantification. For the determination of cadmium, the preconcentration step was carried out

by applying a potential of -1.4 V for 30 s, while that for the determination of mercury, the preconcentration step was performed by applying a potential of -0.7 V for 30 s. The anodic stripping curves were recorded and the stripping peak currents were considered as the analytical signals. Several known amounts of Cd^{2+} and Hg^{2+} were added to the sample solutions (with unknown concentration) to perform the metal determination by the standard additions method.

Preparation of TPNP-Cd-1, TPNP-Cd-2 and TPNP-Cd-3

The cadmium-modified nanoparticles were prepared as follows; 40 mg of TPNP were added to 17 ml of a water solution containing 52 mg of cadmium (II) nitrate tetrahydrate (0.17 mmoles) and the resulting mixture was stirred at 50ºC for 24 h. Then, the final mixture was centrifuged (10000 rpm, 5 m), the solid precipitate was washed three times with 5 mL of ultrapure water and the nanoparticles were dried under vacuum overnight yielding TPNP-Cd-1**.** Similarly, TPNP-Cd-2 and TPNP-Cd-3 were synthesized but using cadmium (II) acetate dihydrate (45 mg, 0.17 mmoles) or cadmium (II) acetylacetonate (53 mg, 0.17 mmoles), respectively.

.- TPNP-Cd-1

IR (cm^{-1})**: 3421** s, br, $\nu_{(OH)}$; **2960** vw, $\nu_{(CH)}$ ÷**1626** m, br, $\delta_{(HOH)}$; **1225 s**h, m, $\delta_{(POH)}$; **1032** vs, vbr, $\nu_{(P=O)}$; **797** m; **645** m; **580** m, $\delta_{(O\text{-}P\text{-}OH)}$; **513** m $\rho_{(PO2)}$. (Fig. 1 and Fig.7)

^{31}P MAS NMR (δ in ppm) broad signal from +8 to -33 with peaks at **-20** ($(HPO_4)^{2-}$) and **-28** ($(PO_4)^{3-}$). (Fig. 2)

DRX. 2θ (plane) **14.6** (012); **18.1**; **20.4-20.9** (104/110); **24.4** (113); **29.4** (024); **32.6** (116/211); **36.7** (300); **50.0** (226); **53.6** (137); **57.5** (410). (Fig. 3)

.- TPNP-Cd-2

IR (cm^{-1})**: 3441** s, br, $\nu_{(OH)}$; **2960** vw, $\nu_{(CH)}$; **1621** m, br, $\delta_{(HOH)}$; **1220 s**h, m, $\delta_{(POH)}$; **1023** vs, vbr, $\nu_{(P=O)}$; **802** m; **640** m; **581** m, $\delta_{(O-P-OH)}$; **540** m. (Fig. 1)

^{31}P MAS NMR (δ in ppm) broad signal from +19 to -34 with peaks at +**3**, **-20** ($(HPO_4)^{2-}$) and **-28** ($(PO_4)^{3-}$). (Fig. 2)

DRX. 2θ (plane) **20.9** (too intense to be 110); **24.3** (113), **27.5**; **29.1** (024); **31.5**; **36.6** (300); **46.7** (128); **49.7** (226); **53.6** (137); **57.4** (410). (Fig 3)

.- TPNP-Cd-3

IR (cm^{-1})**: 3421** s, br, $\nu_{(OH)}$; **2960** vw, $\nu_{(CH)}$ -; **1621** m, br, $\delta_{(HOH)}$; **1215 s**h, m, $\delta_{(POH)}$; **1025** vs, vbr, $\nu_{(P=O)}$; **802** m; **638** m; **581** sh, m, $\delta_{(O-P-OH)}$; **547** m. (Fig. 1)

^{31}P MAS NMR (δ in ppm) broad signal from +18 to -34 with clear peaks at +**4**, **-20** ($(HPO_4)^{2-}$) and **-27** ($(PO_4)^{3-}$) (Fig. 2)

DRX. 2θ (plane) **20.9** (too intense to be 110); **24.2** (113), **29.3** (024); **32.4** (too intense to be 116/211); **36.6** (300); **44.6** (223); **46.6** (128); **49.7** (226); **53.6** (137); **57.3** (410). (Fig. 3)

Preparation of TPNP-Hg-1 and TPNP-Hg-2

The mercury-modified nanoparticles were prepared as described above for TPNP-Cd; 40 mg of TPNP were added to 17 ml of a water solution containing 58 mg of mercury (II) nitrate monohydrate (0.17 mmoles) and the resulting mixture was stirred at 50ºC for 24 h. Then, the final mixture was centrifuged (10000 rpm, 5 m), the solid precipitate was washed three times with 5 mL of ultrapure water and the nanoparticles were dried under vacuum overnight yielding TPNP-Hg-1. In a similar way TPNP-Hg-2 were synthesized but using mercury (II) acetate (54 mg, 0.17 mmoles)

.- **TPNP-Hg-1**

IR (cm^{-1})**: 3431** s, br, $\nu_{(OH)}$; **2960** vw, $\nu_{(CH)}$ **2921**vw $\nu_{(CH)}$ (docusate sodium salt); **1617** m, br, $\delta_{(HOH)}$; **1258** m; **1018** vs, vbr, $\nu_{(P=O)}$; **797** m; **635** m; **522** m. (Fig. 4)

^{31}P MAS NMR (δ in ppm) broad signal from +35 to -35 with peaks at +**16**, +**5**, **0, -17** and **-28** ($(PO_4)^{3-}$). (Fig. 4)

DRX. 2θ (plane) **21.1**(110); **24.5** (113); **32.7** (too intense to be 116/211). (Fig. 5)

.- **TPNP-Hg-2**

IR (cm^{-1})**: 3421** s, br, $\nu_{(OH)}$; **2960** vw, $\nu_{(CH)}$; **2921**vw $\nu_{(CH)}$; **1611** m, br, $\delta_{(HOH)}$; **1258** m; **1018** vs, vbr, $\nu_{(P=O)}$; **797** m; **635** m; **532** m. (Fig. 4)

^{31}P MAS NMR (δ in ppm) broad signal from +20 to -35 with peaks at +**6**, +**1, -17** and **-27** ($(PO_4)^{3-}$). (Fig. 4)

DRX. 2θ (plane) **24.2**(113); **31.1** ; **32.4** (too intense to be 116/211). (Fig. 5)

The protonation of TPNP-Cd-2 and TPNP-Hg-2

To protonate metal-modified nanoparticles, 80 mg of TPNP-Cd-2 were added to 5 mL of a 0.1 M HCl aqueous solution and the mixture was centrifuged at 10000 rpm for 60 s. The resultant solid TPNP-Cd-2-H was washed (by centrifugation) three times with 5 mL of ultrapure water, and then dried at r.t. overnight. TPNP-Hg-2-H was obtained and purified in a similar way.

.- **.- TPNP-Cd-2-H**

IR (cm^{-1})**: 3431** s, br, $\nu_{(OH)}$; **2960** vw, $\nu_{(CH)}$; **1626** m, br, $\delta_{(HOH)}$; **1033** vs, vbr, $\nu_{(P=O)}$; **802** m; **640** m; **581** m, $\delta_{(O\text{-}P\text{-}OH)}$; **513** m $\rho_{(PO2)}$. (Fig. 6)

^{31}P MAS NMR (δ in ppm) broad signal from +8 to -34 with peaks at **0**, **-5** ($(H_2PO_4)^-$)**, -13** ($(H_2PO_4)^-$)**, -21** ($(HPO_4)^{2-}$) and **-27** ($(PO_4)^{3-}$). (Fig. 6)

DRX. 2θ (plane) **14.6 (**012**); 20.2 (**104); **21.0** (110); **24.4 (**113**); 29.4 (**024**); 32.6 (**116/211**); 36.8 (**300**); 47.0 (**128**); 50.0 (**226**); 53.9 (**137**); 57.6 (**410**)** (Fig. 6)

.- **TPNP-Hg-2-H**

IR (cm^{-1})**: 3441** s, br, $\nu_{(OH)}$; **2960** vw, $\nu_{(CH)}$; **1631** m, br, $\delta_{(HOH)}$; **1038** vs, vbr, $\nu_{(P=O)}$; **797** m; **640** m; **581**m**,** $\delta_{(O-P-OH)}$; **513** m $\rho_{(PO2)}$. (Fig. 6)

^{31}P MAS NMR (δ in ppm) broad signal from +8 to -35 with peaks at +**3**, **0**, **-5** ($(H_2PO_4)^-$)**, -13** ($(H_2PO_4)^-$)**, -21** ($(HPO_4)^{2-}$) and **-28** ($(PO_4)^{3-}$). (Fig. 5)

DRX. 2θ (plane) **14.6 (**012**); 18.1; 21.5; 24.5 (**113**); 28.2; 29.5 (**024**); 31.5; 32.8 (**too intense to be 116/211**); 40.3; 43.8; 46.2; 52.9; 58.2.** (Fig. 5)

Preparation of NPFT-Cd-1-OA.

To prepare N-octylamine-modified nanoparticles, 50 mg of TPNP-Cd-1 were added to 3 mL of a N-octylamine solution (60 μL, 0.37 mmol) in a mixture ethanol/water (50%, v/v) and the resultant dispersion was stirred 48 h at room temperature. Afterwards, the resultant solid TPNP-Cd-1-OA was washed (by centrifugation) three times with 5 mL of ultrapure water, three times with 5 mL of an ethanol/water mixture (50%, v/v) and finally dried at r.t. overnight.

.- **NPFT-Cd-1-OA**

IR (cm^{-1})**: 3421** s, br, $\nu_{(OH)}$; **3176** s**,** b, $\nu_{(NH)}$; **2950** s, $\nu_{(CH)}$; **2920** s, $\nu_{(CH)}$; **2852** s, $\nu_{(CH)}$; **1631** m, br, $\delta_{(HOH)}$; **1570** sh, $\delta_{(RNH3)}$; **1469** m, $\delta_{(HCH)}$ **; 1293** m; **1230** sh, $\delta_{(POH)}$; **1060,** sh, $\nu_{(P=O)}$; **1023** vs, br, $\nu_{(P=O)}$; **802** w; **724** w; **640** w; **550** m**.** (Fig. 7)

^{13}C CP/MAS NMR (δ in ppm) **: 15, 24, 29, 31, 33, 41.** (Fig. 7)

^{31}P MAS NMR (δ in ppm) broad signal from +8 to -40 with peaks at **-3**, **-21** ($(HPO_4)^{2-}$) and **-28** ($(PO_4)^{3-}$). (Fig. 8)

DRX. 2θ (plane) **14.5** (012); **20.9** (110); **24.3** (113); **29.4** (024); **32.5** (116/211); **36.5** (300); **46.8** (128); **49.8** (226); **53.9** (137); **57.3** (410). (Fig. 8)

The protonation of TPNP-Cd-1-OA

To protonate octylamine-modified nanoparticles, 80 mg of TPNP-Cd-1-OA were added to 5 mL of a 0.1M HCl solution and the mixture was centrifuged at 10000 rpm for 60 s. The resultant solid, TPNP-Cd-1-OA-H, was washed (by centrifugation) three times with 5 mL of ultrapure water, and then dried at r.t. overnight.

.-**TPNP-Cd-1-OA-H**

IR (cm^{-1})**: 3411** s, br, $\nu_{(OH)}$; **3186** m**,** b, $\nu_{(NH)}$; **2960** s, $\nu_{(CH)}$; **1626** m, br, $\delta_{(HOH)}$; **1464**m, $\delta_{(HCH)}$**;** **1220** sh, $\delta_{(POH)}$; **1028** vs, br, $\nu_{(P=O)}$; **640** w; **581** w, $\delta_{(O-P-OH)}$; **513** m $\rho_{(PO2)}$. (Fig. 8)

^{31}P MAS NMR (δ in ppm) broad signal from +8 to -40 with peaks at **-3**, **-21** ($(HPO_4)^{2-}$) and **-28** ($(PO_4)^{3-}$). (Fig. 8)

DRX. 2θ (plane) **14.5** (012); **20.3** (104); **20.9** (110); **24.4** (113); **29.4** (024); **32.5** (116/211); **36.7** (300); **47.0** (128); **49.8** (226); **53.9** (137); **57.5** (410). (Fig. 8)

RESULTS AND DISCUSSION

Titanium phosphate nanoparticles, TPNP, were obtained following a procedure previously described in the literature[25,34] and explained elsewhere[37,38]. Typically, 5.65 mmol of AOT was dissolved into 12.5 g of ethanol and then H_3PO_4 (51 mmol) was added. After stirring for 3 h. at r.t., the solution was filtered and the precipitate was removed. Then, a mixture of TBOT in ethanol (2.5mmol/15.5 mL) was fast dropped into the filtered solution, and stirred at 80 ºC for 6 h. A white solid product was obtained and washed with ethanol and diethyl ether for several times until neutral pH and then dried at 80 ºC overnight. They were characterized by TEM (Fig. S-1), XRD (Fig. S-2), ^{1}H MAS NMR (Fig. S-3), ^{31}P CPMAS NMR (Fig. S-4), and FTIR (Fig. S-5). The obtained data are

practically coincident with those of the reported titanium phosphate nanoparticles.[25,34] The most noticeable difference is that TPNP have a smaller diameter (30±5 vs. 50 nm).

The infrared spectrum of TPNP (Fig. S-5) deserves a detail analysis. It shows two broad bands at 3431 ($\nu_{(OH)}$) and 1631 cm^{-1} ($\delta_{(HOH)}$) attributable to the physically adsorbed water, and a weak signal at 2960 cm^{-1} (alkyl $\nu_{(CH)}$) due to DOSS, the surfactant used for the synthesis of TPNP, both of them were also detected by proton solid NMR (Fig. S-3).[25] It also exhibits a band at 635 cm^{-1} that is present in the IR spectrum of $NaTi_2(PO_4)_3$,[39] the crystalline component of TPNP identified by its XRD signals (Fig. S-2).[25,39] In addition to the very strong and broad band at about 1028 cm^{-1} ($\nu_{(P=O)}$) associated to the phosphate groups, the IR spectrum shows some other interesting peaks: a shoulder at 1227 cm^{-1} ($\delta_{(POH)}$) attributable to the dihydrogenphosphate groups;[40,41] a band of medium intensity about 510 cm^{-1} (ρ_{PO2}) also due to the dihydrogenphosphate groups;[42] and a peak of weak intensity at 581 cm^{-1} ($\delta_{(O\text{-}P\text{-}OH)}$) attributable to the hydrogenphosphate groups.[43–45] The presence of phosphate, hydrogen phosphate and dihydrogen phosphate groups in TPNP is confirmed by its ^{31}P CPMAS NMR spectrum (Fig. S-4).[25] We have found that the intensity of the bands at 581 cm^{-1} ($\delta_{(O\text{-}P\text{-}OH)}$) and at 510 cm^{-1} ($\rho_{(PO2)}$), due to the acid phosphates, are very sensitive to the proton exchange process and, therefore, very useful to follow the incorporation/release of cations and amines to/from the TPNP. Finally, the broad band at 2930 cm^{-1} ($\nu_{(OH)}$) is due to the POH groups[41,44], while the signal at 2381 cm^{-1} seems to be a combination band.[44]

The ^{31}P CP/MAS NMR spectrum of TPNP (Fig. S-4) closely resembles that one reported by Liu et al.[25], but the chemical shifts (-27.9, -20.6, -13.8 and -6.0 ppm) are not exactly the same. They assumed that the peaks at -26.4, -19.1 and -10.9 ppm, are due to $(PO_4)^{3-}$, $(HPO_4)^{2-}$ and $(H_2PO_4)^{-}$ groups, respectively, but a fourth peak at about -4 ppm was not assigned. In order to obtain more information about the origin of this band, additional solid state NMR measurements were performed. In the case of ^{31}P NMR, there is no need to use the CP method to improve the spectral signal-to-noise ratio, but this type of experiments could provide some insights to the molecular structure of the

TPNPs. Thus, a series of spectra varying the CP contact time between ^{1}H and ^{31}P were acquired. The kinetics of the CP for the four resonances is illustrated in Fig. S-6 and the results summarized in Table S-1. It is observed that $T_{1\rho}$ (^{1}H) and T_{HP} decrease with increasing number of protons, suggesting that the peak at -6 ppm corresponds to a protonated phosphate. Generally, solids with abundant and strongly coupled protons exhibit a uniform response, i.e., a single value of $T_{1\rho}$ (^{1}H) independently of their surroundings. In our case, the values of $T_{1\rho}$ (^{1}H) indicate some differences in the proton environments cross-polarizing with each of the four ^{31}P resonances; although the values associated to peaks at -6 and -13.8 ppm are similar. Also, the values of the CP time constant T_{HP}, which decreases with decreasing ^{1}H-^{31}P distances or increasing number of protons, suggest an increasing protonation of phosphorous compounds with increasing chemical shift, backing the previous statement.

In addition, we recorded two ^{31}P MAS NMR spectra of TPNP, with ^{1}H and without ^{1}H decoupling (Fig. S-7) to seek further evidence to support the above assumption. Unexpectedly, both of them exhibit an extra peak at 0 ppm, assignable to H_3PO_4, probably originated by hydrolysis of the phosphate groups in the TPNP either by the water retained in its surface (detected by IR and proton solid NMR) or by the water present in the atmosphere. This hydrolysis will be discussed later. The pattern of the spectra is markedly different of that one obtained by the ^{31}P CPMAS NMR method (Fig. S-4), although the chemical shifts are practically coincident. As it could be anticipated, the spectra collected (Fig. S-7) show the same intensity in the bands due to the PO_4^{3-} groups, but different for acid phosphates (it is expected higher intensity for the bands due to HPO_4^{2-} and $H_2PO_4^{-}$ groups in the spectrum obtained with ^{1}H decoupling). This means that the signal at -6 ppm should be attributable to a dihydrogenphosphate. However, it should be pointed out that this assignment is not as straightforward as it could be desirable due to variations in the Ti-O-P coordination, the presence of Na^{+}, as well as changes in bond angles and bond lengths which could modify the values of the observed chemical shifts to some extent[46].

279 Nevertheless, the characterization of the products obtained from TPNP by cation exchange
280 with Cd^{2+} and Hg^{2+}, confirm that this assignation is correct (discussed later).

281 The formation of H_3PO_4 inside the TPNP was not detected previously because the ^{31}P NMR
282 spectra of the samples were obtained using the ^{31}P CPMAS/NMR technique, which is not able to
283 detect free molecules with certain mobility like phosphoric acid. Fig. S-8a shows two ^{31}P MAS NMR
284 spectra of the same TPNP sample; one was recorded just after the preparation, the other one a week
285 later. The spectra were edited in such a way that the intensity of the peak at -28 ppm has the same
286 intensity in both spectra. In the second spectrum, recorded after seven days, it is not only observed
287 the occurrence of a new signal at 0 ppm, assigned to H_3PO_4, but also that the intensity of all other
288 peaks has increased, suggesting that all the phosphates groups (PO_4^{3-}, HPO_4^{2-} and $H_2PO_4^-$) have
289 followed a hydrolysis process. The spectrum of TPNP after four months in open air (Fig. S-8b)
290 evidences that the hydrolysis of the TPNP is a complicated process; the band at -13 ppm has been
291 split into two closed peaks, at -12 and -14 ppm, and the signal at -20 ppm appears now at -21 ppm[47].

292 As could be expected, the hydrolysis of TPNP is very fast in liquid water and the resultant
293 phosphoric acid is accumulated in the solvent, as it is evidenced in the ^{31}P NMR spectrum of TPNP
294 in D_2O after stirring the nanoparticles in deuterated water for 10 minutes at room temperature (Fig.
295 S-9). Since the incorporation of metallic cations Cd^{2+} and Zn^{2+} into TPNP have been carried out in
296 water at 50º for 24 h,[34] the existence of a competitive reaction like the hydrolysis of the nanoparticles
297 could be a problem. However, if 40 mg of TPNP are added to 17 ml of a water solution containing
298 0.17 mmol of $Cd(NO_3)_2$ only tiny amounts of phosphoric acid are detected in the solution after 2h at
299 50ºC (Fig. S-10). Since separate experiments clearly indicate that the hydrolysis is very fast at the
300 beginning and later it slows down it seems that when the nanoparticles are added onto water solution
301 of the metallic ion, the exchange reaction is much faster than the hydrolysis. On the contrary, a
302 minute hydrolysis in the starting material, TPNP, did not affect the properties of the nanoparticles
303 obtained after incorporation of metal ions, as far as we were able to detect.

Incorporation of Cadmium (II) cations

The insertion of Cd^{2+} into TPNP has been described previously.[34] In order to control the cadmium (II) concentration inside the resulting nanoparticles, we repeated the reaction following the same procedure with slight modifications. Briefly, we dispersed 40 mg of TPNP in 17 ml of a water solution containing 0.17 mmol of $Cd(NO_3)_2$ and stirred the mixture at r.t. for 24 h (reaction I). Then, we doubled the amount of Cadmium (II), maintaining the room temperature (reaction II). Finally, we duplicated the amounts used in reaction I, but stirring the resulting suspension at 50ºC (that is, following closely the recipe explained in the literature,[34] reaction III). The characterization with FTIR and TEM of the nanoparticles TPNP-Cd-I, TPNP-Cd-II and TPNP-Cd-III obtained in reactions I, II and II, respectively, showed that they were almost identical, within the margin error of the techniques. Particularly interesting were the EDS (TEM) data; they indicated that the relative concentration of Cd^{2+} in the nanoparticles is essentially coincident in the three cases. These facts suggest that the substitution of hydrogen ions in TPNP follows a pattern similar to that exhibited by $Ti(HPO_4)_2$,[7] that is, some of the protons are easily substituted by Cd^{2+} but for further substitution a more basic environment is required (see introduction). This result prompted us to modify our strategy to increase the concentration of metal ions inside the titanium phosphate nanoparticles. Thus, considering that in these reactions the final suspension is acid (pH=2.47 at the end of reaction III) as a consequence of the ion exchange (protons of acid phosphates are replaced by Cd^{2+} cations), we decided to use cadmium (II) acetate and cadmium (II) acetylacetonate salts instead of $Cd(NO_3)_2$ as source of Cd^{2+} ions. Since these basic anions (CH_3COO^- and $[CH_3COCHCOCH_3]^-$) will increase the solution pH, their presence should shift the equilibrium inducing a higher incorporation of metal cations into the TPNP.

Therefore, we added 40 mg of TPNP to a 17 ml of water solution containing 0.17 mmol of the cadmium salts ($Cd(NO_3)_2 \cdot 4H_2O$; $Cd(CH_3COO)_2 \cdot 2H_2O$ and $Cd(C_2H_7O_2)_2$) and then stirred the

resulting mixtures for 24 h at 50ºC, obtaining TPNP-Cd-1, TPNP-Cd-2 and TPNP-Cd-3 respectively. The TEM micrographs revealed that the obtained nanoparticles retain roughly the spherical shape and the diameter size of the starting TPNP (Fig. S-11). According to our expectations, the pH of the final reaction mixtures, shown in the last column of Table 1, increases when passing from nitrate through acetate to acetylacetonate cadmium (II) salts. Consequently, the higher the basicity of the anion used, the greater is the amount of incorporated cadmium (II) ions into the resulting nanoparticles, as pointed out by the EDS (TEM) data of the prepared nanoparticles (see Table 1).

Comparing the infrared spectra of phosphate nanoparticles containing cadmium (II) cations with that of the starting TPNP it is easy to see small modifications, the most relevant are in the 700-400 cm^{-1} region (Fig. 1). In the IR spectrum of TPNP-Cd-1 the band ca. 510 cm^{-1}, attributed to the $H_2PO_4^-$ groups, has lower intensity than the same band in the IR spectrum of TPNP. Simultaneously, the bands at -6 and -13 ppm of the ^{31}P spectrum of the starting material, also due to the dihydrogenphosphate groups, have practically disappeared in the ^{31}P spectrum of TPNP-Cd-1(Fig. 2). This is easily understandable taking into account that the protons of the dihydrogenphosphate groups are more acidic that the proton of the HPO_4^{2-} moieties, and, therefore, they will be the first to be substituted by the incoming Cd^{2+} cations. Incidentally, the simultaneous fading of the peaks at -6 and -13 ppm in the phosphorus NMR spectra of TPNP-Cd-1 reinforces the assignation of the band at -6 ppm in the ^{31}P spectrum of TPNP to the $H_2PO_4^-$ groups. There is not any band ca. 510 cm^{-1} in the 700-400 cm^{-1} region of the IR spectra corresponding to TPNP-Cd-2 and TPNP-Cd-3, although a new band around 540-547 cm^{-1} (Fig.1) is observed. Similarly, a new signal in the ^{31}P MAS NMR spectra of the nanoparticles containing more cadmium (II) ions was detected, namely that at 3-4 ppm. These new signals observed both in the IR and the ^{31}P spectra suggest the formation of cadmium phosphates. Interestingly, the bands due to $NaTi_2(PO_4)_3$ and to the hydrogenphosphate groups in the infrared spectra (those at 640 and 580 cm^{-1}), as well as in the ^{31}P MAS NMR spectra (those at -28

and -20 ppm) are present in all the spectra, suggesting that the HPO_4^{-2} moieties and the crystalline nucleus of the starting material remain mainly unaltered along the substitution process.

However, comparing the XRD patterns of these cadmium derivatives with that of the starting TPNP (Fig. 3), it can be seen that the successive incorporation of Cd^{2+} ions leads to a progressive crystal destruction (although the peaks corresponding to some crystal planes of $NaTi_2(PO_4)_3$ are recognizable in all the patterns). Furthermore, the intensity of the peaks at 2θ = 20.9 and 32.4 (corresponding to the planes (110) and (116)/(211) respectively) have an unusual intensity in the XRD patterns of TPNP-Cd-2 and TPNP-Cd-3. On the other hand, new peaks appear 2θ = 18.1 and 27.5 and 31.5 in the XRD patterns of TPNP-Cd-1 and TPNP-Cd-2. The profound modifications of the original XRD pattern as the metal ions are incorporated into the TPNP nanoparticles evidence that this process is not a simple ion exchange procedure since the crystalline nucleus, which is highly reactive[28,29,31,32], is also affected. The alterations in the $NaTi_2(PO_4)_3$ were also detected by luminescence measurements;[33] in fact, the area under the fluorescence signal at 720 nm diminishes when passing from TPNP to TPNP-Cd-3 (Fig. S-12)

Incorporation of Mercury (II) cations

The Hg^{2+} ions were also introduced inside the TPNP following a procedure similar to that described for the insertion of cadmium (II) ions into the titanium phosphate nanoparticles. Thus, we added 40 mg of TPNP to 17 ml of a water solution containing 0.17 mmol of the mercury salts ($Hg(NO_3)_2.2H_20$ and $Hg(CH_3COO)_2$, and then stirred the resulting mixtures for 24 h at 50ºC, obtaining TPNP-Hg-1 and TPNP-Hg-2 respectively. Again, the obtained nanoparticles retain the spherical shape and the diameter size of the starting TPNP, as revealed by the TEM micrographs shown in Fig. S-13. However, in this occasion, some dark spots inside each nanoparticle are observed. A detailed examination by EDS (TEM) indicated that the mercury ions are concentrated in these dots. As expected, the utilization of mercury (II) acetate instead of mercury (II) nitrate yields

higher concentration of the metal ions in the obtained nanoparticles, and higher pH values in the final mixture solution (see Table 2).

The region between 700 and 400 cm^{-1} in the infrared spectra of TPNP-Hg-1 and TPNP-Hg-2, as well as their ^{31}P MAS NMR spectra, are shown in Fig. 4. The disappearance of the peaks at 580 and at 510 cm^{-1} (in the infrared spectra) and the bands at -6, -13 and -20 ppm (in the ^{31}P spectra), all of them attributable to the acid phosphate groups, clearly indicate that the protons of the dihydrogenphosphates and hydrogenphosphates have been substituted by the mercury cations. The presence of new signals in the infrared spectra (at 522 and 532 cm^{-1}, respectively) and in the NMR spectra (at -17, 0, +5 and +16 ppm and at -17,+1, and +6 ppm, respectively) should correspond to the formation of mercury phosphates. On the other hand, the persistence of the peaks at 635 cm^{-1} (in the IR spectra) and -28 ppm (in the solid NMR spectra), both due to phosphate groups, suggests the perseverance of the $NaTi_2(PO_4)_3$ nucleus. However, the XRD patterns of mercury derivatives (Fig. 6) indicate clearly the loss of crystallinity of that nucleus, suggesting that the incorporation of metal ions into TPNP is not a simple proton/metal ion exchange, but it affects all the components of the nanoparticle. The alterations in the $NaTi_2(PO_4)_3$ were again detected by luminescence measurements (Fig. S-14)

The protonation of the nanoparticles containing metal ions

The usefulness of TPNP as labels for electrochemical biosensors rests in the possibility of rapidly releasing the metal ions incorporated into the nanoparticle to be detected by the corresponding electrodes. In order to verify the availability of metallic ions from TPNP-Cd-2 and TPNP-Hg-2, these nanoparticles were treated with a water solution of HCl 0.1 M for 60 s yielding TPNP-Cd-2-H and TPNP-Hg-2-H respectively. (See experimental part for details).

The new nanoparticles were characterized by IR, solid state NMR, TEM and XRD techniques. They preserve approximately the size and shape of the parent nanoparticles, but EDS (TEM) data

reveals that the cadmium (II) cations have not been totally released. In fact, carefully monitoring of the process indicates that neither Cd^{2+} nor Hg^{2+} were completely released (see later). The appearance of the bands at 581 and 513 cm^{-1} in their infrared spectra and the signals at -5, -13 and -21 ppm in their ^{31}P MAS NMR spectra indicates that some hydrogenphosphates and dihydrogenphosphates have been reconstituted (see Fig. 6), that is, the protons have replaced most of the metal ions. However, the broad bands observed in the range 0 - 3 ppm in their phosphorus spectra, their XRD patterns (Fig 5) and their fluorescence signals (Fig S-16), clearly show that the starting material, namely TPNP, is not recovered.

It is possible to monitor the abundance of the metal cations in solution along the entire ion-exchange process, that is, in the formation of TPNP-Cd-2 and TPNP-Hg-2 and in the subsequent M^{2+} release in acid media. A voltammetric technique using the standard additions method described in the Experimental section was employed. As illustrated in Fig. S-17 and Fig. S-18, the synthesis of the titanium phosphate nanoparticles containing Cd^{2+} and Hg^{2+} have been carried out in the presence of metal ions excess. On the other hand, the release of the Cd^{2+} or Hg^{2+} cations incorporated in the nanoparticles is not complete after 60 s in acid media, the time used in the analytical applications. The release of M^{2+} is complete after 24 h elapsed.

Incorporation of N-octylamine

The application of the titanium phosphate nanoparticles as labels for electrochemical biosensors requires the immobilization of proteins on their surface.[25,34] To this end, the nanoparticles, already loaded with metal cations, were treated successively with PAH (poly (allylamine hydrochloride)) glutaraldehyde and the desired protein.[25,34] Since these nanoparticles were able to react with the poly (allylamine hydrochloride), it is likely that they could also react directly with the amine groups of the proteins. However, considering that the TPNP/protein interaction would be very difficult to characterize, it seems convenient to study first the reaction between an amine and the

titanium phosphate nanoparticles. The elected amine was N-octylamine, not only because it possesses a high number of CH_2 groups, easily detected by IR and ^{13}C NMR, but also because it is only partially soluble in water and therefore the resultant solution is not too basic to dissolve the TPNP. Thus, TPNP-Cd-1 was treated with N-octylamine in ethanol/water (v/v, 50%) to yield TPNP-Cd-1-OA, nanoparticles of shape and size closed to those of the starting material. The infrared spectrum of TPNP-Cd-1 shows remarkable differences with that of the new nanoparticles (see Fig. 7). In the IR spectrum of TPNP-Cd-1-OA the bands at 2950 cm^{-1}, $\nu_{(CH)}$; 2920 cm^{-1}, $\nu_{(CH)}$; and 2852 cm^{-1}, $\nu_{(CH)}$, and that at 1469 cm^{-1}, $\delta_{(HCH)}$, clearly indicates the presence of the amine CH_2 groups in the new material. On the other hand, the absence of the band at 513 cm^{-1}, $\rho_{(PO2)}$, due to the dihydrogenphosphate groups, the shoulder at 1570 cm^{-1} (δ-RNH_3^+) and the appearance of a broad signal at 3176 cm^{-1} (ν-RNH_3^+) suggest the formation of a phosphate/ammonium ion pair. This hypothesis is also supported by the ^{13}C MAS NMR spectrum of TPNP-Cd-1-OA (see Fig. 7), closely related to that of N-octylammonium tetrafluoroborate[48]. The ^{31}P MAS NMR spectrum of the new nanoparticles exhibits a new band ca. -3 ppm and its XRD pattern retains most of the signals corresponding to TPNP-Cd-1 (see Fig 8) but these data do not provide relevant structural information.

The formation of amine/phosphate ion pairs by direct reaction opens the possibility to attach proteins to the titanium phosphate nanoparticles in a simple way, facilitating the preparation of this kind of electrochemical biosensors.

It is also noteworthy the comparison of the infrared spectra in the region 4000-2800 cm^{-1} of the nanoparticles TPNP-Cd-X-OA (X=1-3), the resulting products from the reaction of TPNP-Cd-X (X=1-3) with N-octylamine in ethanol/water (v/v, 50%) and collected in Fig. 8. This image shows that the higher the concentration of Cd^{2+}, the lower the intensity of the signals at 2960, 2921 and 2852 cm^{-1}, $\nu_{(CH)}$, corresponding to amine CH_2 groups. That is, the increasing incorporation of metal ions leads to a decreasing amount of N-octylamine in the new nanoparticles. This is understandable

taking into account that the metal ions and the amine compete for the protons of the acid phosphates, the first to replace them, and the second for the formation of phosphate/octylammonium ion pairs.

The protonation of the nanoparticles containing metal ions and amines

The final step in the application of electrochemical biosensors based in titanium phosphate nanoparticles consists in the release of the metallic cations from nanoparticles containing both metal ions and proteins. In this regard, we treated TPNP-Cd-1-OA with 0.1 M HCl during 60 s, obtaining TPNP-Cd-1-OA-H as nanoparticles with the habitual shape (spherical) and size (diameter about 30 nm). Again, the release of cadmium ions is incomplete (the percentage of Cd in the nanoparticle decreases from 1.66 to 0.42 %, according to EDS data). On the other hand, TPNP-Cd-1-OA-H recovers some hydrogenphosphates and dihydrogenphosphates, as indicated by the band at 581 cm^{-1}, $\delta_{(O\text{-}P\text{-}OH)}$ and 513 cm^{-1}, $\rho_{(PO2)}$, respectively, in its IR spectrum, but the nanoparticle is not identical to the starting TPNP as evidenced by its ^{31}P NMR and XRD patterns (bottom of Fig. 8).

Conclusions

The TPNP is hydrolyzed in presence of H_2O. However, this process is slower than the proton/cation exchange even when the reaction is carried out in warm water. It is possible to incorporate different amounts of metal ions into TPNP using distinct metal salts, taking advantage of the different basicity of the counterions. A detailed analysis of these reactions indicates that they also affect the crystalline nucleus of the nanoparticles and, therefore, they do not consist in a simple ion exchange process. N-octylamine can be attached to the titanium phosphate nanoparticles containing Cd^{+2} ions by direct reaction, forming phosphate/N-octylammonium ion pairs. Most of the incorporated metal cations and N-octylamine are removed by treating the corresponding nanoparticles with 0.1 M hydrochloric acid aqueous solution during only 60 s, explaining satisfactorily why the TPNP can be used as labels for electrochemical biosensors.

ASSOCIATED CONTENT

Supporting Information. Figures and tables showing additional characterization data of nanostructured materials from several techniques as IR, NMR, TEM or fluorescence.

AUTHOR INFORMATION

Corresponding Author

* Francisco J. García Alonso, e-mail: fjga@uniovi.es.

Notes

The authors declare no competing financial interest.

ACKNOWLEDGMENTS

This work has been supported by the FC-15-GRUPIN-021 project from the Asturias Regional Government and the CTQ2014-58826-R project from the Spanish Ministry of Economy and Competitiveness (MEC). Daniel Martín-Yerga thanks the MEC for the award of a FPI grant (BES-2012-054408). Leoncio Garrido acknowledges financial support provided by CSIC. We thank the technician Isabel Cancelo for the synthesis of the starting material.

REFERENCES

1. R. Murugavel, A. Choudhury, M. G. Walawalkar, R. Pothiraja, and C. N. R. Rao, *Chem. Rev.*, 2008, **108**, 3549–3655.

2. R. Lin and Y. Ding, *Materials (Basel).*, 2013, **6**, 217–243.

3. R. Llavona, M. Suarez, J. R. Garcia, and J. Rodriguez, *Inorg. Chem.*, 1989, **28**, 2863–2868.

4. A. Bhaumik and S. Inagaki, *J. Am. Chem. Soc.*, 2001, **123**, 691–696.

5. B. B. Sahu and K. Parida, *J. Colloid Interface Sci.*, 2002, **248**, 221–230.

6. Q. Wang, L. Zhong, J. Sun, and J. Shen, *Chem. Mater.*, 2005, **17**, 3563–3569.

7. K. Jia, B. Pan, Q. Zhang, W. Zhang, P. Jiang, C. Hong, B. Pan, and Q. Zhang, *J. Colloid Interface Sci.*, 2008, **318**, 160–166.

8. K. Jia, B. Pan, L. Lv, Q. Zhang, X. Wang, B. Pan, and W. Zhang, *J. Colloid Interface Sci.*, 2009, **331**, 453–457.

9. J. Peng, L.-N. Feng, Z.-J. Ren, L.-P. Jiang, and J.-J. Zhu, *Small*, 2011, **7**, 2921–2928.

10. A. Clearfield and D. S. Thakur, *Appl. Catal.*, 1986, **26**, 1–26.

11. F. A. H. Al-Qallaf, L. F. Hodson, R. A. W. Johnstone, J. Y. Liu, L. Lu, and D. Whittaker, *J. Mol. Catal. A Chem.*, 2000, **152**, 187–200.

12. S. M. Patel, U. V. Chudasama, and P. A. Ganeshpure, *React. Kinet. Catal. Lett.*, 2002, **76**, 317–325.

13. S. M. Patel, U. V. Chudasama, and P. A. Ganeshpure, *J. Mol. Catal. A Chem.*, 2003, **194**, 267–271.

14. J. Liu, J. Zhang, S. Cheng, Z. Liu, and B. Han, *Small*, 2008, **4**, 1976–1979.

15. A. Dutta, A. K. Patra, S. Dutta, B. Saha, and A. Bhaumik, *J. Mater. Chem.*, 2012, **22**, 14094-14100.

16. W. Hogarth, S. Muir, a Whittaker, J. Dinizdacosta, J. Drennan, and G. Lu, *Solid State Ionics*, 2007, **177**, 3389–3394.

17. A. Espina, E. Jaimez, S. A. Khainakov, C. Trobajo, J. R. García, and J. Rodríguez, *Chem. Mater.*, 1998, **10**, 2490–2496.

18. M. Serra, H. G. Baldovi, F. Albarracin, and H. Garcia, *Appl. Catal. B Environ.*, 2016, **183**, 159–167.

19. A. N. Christensen, E. K. Andersen, I. G. K. Andersen, G. Alberti, M. Nielsen, M. S. Lehmann, and T. Tokii, *Acta Chem. Scand.*, 1990, **44**, 865–872.

20. Y. J. Li and M. S. Whittingham, *Solid State Ionics*, 1993, **63–65**, 391–395.

21. A. I. Bortun, L. Bortun, A. Clearfield, M. A. Villa-García, J. R. García, and J. Rodríguez, *J. Mater. Res.*, 1996, **11**, 2490–2498.

22. L. Körösi, S. Papp, and I. Dékány, *Chem. Mater.*, 2010, **22**, 4356–4363.

23. M. V. Maslova, D. Rusanova, V. Naydenov, O. N. Antzutkin, and L. G. Gerasimova, *J. Non. Cryst. Solids*, 2012, **358**, 2943–2950.

24. Y. Bereznitski, M. Jaroniec, A. I. Bortun, D. M. Poojary, and A. Clearfield, *J. Colloid Interface Sci.*, 1997, **191**, 442–448.

25. J. Liu, X. Wei, Y. Yu, J. Song, X. Wang, A. Li, X.-W. Liu, and W.-Q. Deng, *Chem. Commun. (Camb).*, 2010, **46**, 1670–1672.

26. L.-N. Feng, J. Peng, Y.-D. Zhu, L.-P. Jiang, and J.-J. Zhu, *Chem. Commun. (Camb).*, 2012, **48**, 4474–4476.

27. Z. Yin, Y. Sakamoto, J. Yu, S. Sun, O. Terasaki, and R. Xu, *J. Am. Chem. Soc.*, 2004, **126**, 8882–8883.

28. S. Patoux and C. Masquelier, *Chem. Mater.*, 2002, **14**, 5057–5068.

29. S. Il Park, I. Gocheva, S. Okada, and J. Yamaki, *J. Electrochem. Soc.*, 2011, **158**, A1067-A1070.

30. L. Chen, L. Zhang, X. Zhou, and Z. Liu, *ChemSusChem*, 2014, **7**, 2295–2302.

31. N. Hirose and J. Kuwano, *J. Mater. Chem.*, 1994, **4**, 9–12.

32. A. Tsuji, H. Takahashi, and T. Oi, *J. Mater. Chem.*, 2003, **13**, 542–549.

33. S. Nedilko, Y. Hizhnyi, O. Chukova, P. Nagornyi, R. Bojko, and V. Boyko, *J. Nucl. Mater.*, 2009, **385**, 479–484.

34. L.-N. Feng, Z.-P. Bian, J. Peng, F. Jiang, G.-H. Yang, Y.-D. Zhu, D. Yang, L.-P. Jiang, and J.-J. Zhu, *Anal. Chem.*, 2012, **84**, 7810–7815.

35. F. Cheng, T. He, H. Miao, J. Shi, L. Jiang, and J. Zhu, *ACS Appl. Mater. Interfaces*, 2015, **7**, 2979–2985.

36. M. K. Sharma, J. Narayanan, S. Upadhyay, and A. K. Goel, *Biosens. Bioelectron.*, 2015, **74**, 299–304.

37. D. Martín-Yerga, J. Carrasco-Rodríguez, M. B. González-García, F. J. García Alonso, and A. Costa-García, *Electroanalysis*, 2014, **26**, 2574–2579.

38. D. Martín-Yerga, J. Carrasco-Rodríguez, J. L. G. Fierro, F. J. García Alonso, and A. Costa-García, *Electrochim. Acta*, 2017, **229**, 102–111.

39. H. Güler and F. Kurtuluş, *Mater. Chem. Phys.*, 2006, **99**, 394–397.

40. P. L. Stanghellini, E. Boccaleri, E. Diana, G. Alberti, and R. Vivani, *Inorg. Chem.*, 2004, **43**, 5698–5703.

41. J. Xu, D. F.R. Gilson, and I. S. Butler, *Spectrochim. Acta Part A Mol. Biomol. Spectrosc.*, 1998, **54**, 1869–1878.

42. B. J. Rajkumar and V. Ramakrishnan, *Spectrochim. Acta. A. Mol. Biomol. Spectrosc.*, 2001, **57**, 247–254.

43. S. K. Arora, T. R. Trivedi, A. T. Oza, and V. A. Patel, *Acta Mater.*, 2001, **49**, 2103–2107.

44. L. Tortet, J. R. Gavarri, G. Nihoul, and A. J. Dianoux, *J. Solid State Chem.*, 1997, **132**, 6–16.

554 45. K. Rajendran and C. Dale Keefe, *Cryst. Res. Technol.*, 2010, **45**, 939–945.

555 46. C. Schmutz, P. Barboux, F. Ribot, F. Taulelle, M. Verdaguer, and C. Fernandez-Lorenzo, *J. Non. Cryst. Solids*,
556 1994, **170**, 250–262.

557 47. H. Nakayama, T. Eguchi, N. Nakamura, S. Yamaguchi, M. Danjyo, and M. Tsuhako, *J. Mater. Chem.*, 1997, **7**,
558 1063–1066.

559 48. C.-L. Chang, M. Leung, and M.-H. Yang, *Tetrahedron*, 2004, **60**, 9205–9212.

560

561

TABLES AND FIGURES

	O (%)	Na (%)	P (%)	Ti (%)	Cd (%)	pH
TPNP	65,55 (± 4,80)	3,68 (± 0,13)	22,18 (± 3,33)	8,59 (± 1,37)	**0,00**	
TPNP-Cd-1	65,56 (± 1,32)	2,36 (± 0,01)	20,54 (± 1,10)	10,52 (± 0,25)	**1,02 (± 0,03)**	2,47
TPNP-Cd-2	67,39 (± 0,39)	1,59 (± 0,28)	17,04 (± 0,10)	7,26 (± 0,15)	**6,72 (± 0,12)**	4,29
TPNP-Cd-3	62,41 (± 2,96)	2,21 (± 0,33)	18,07 (± 1,20)	7,43 (± 0,60)	**9,88 (± 1,13)**	5,73

Table 1. Relative concentration of O, Na, P, Ti and Cd (EDS (TEM) data) in TPNP, TPNP-Cd-1, TPNP-Cd-2 and TPNP-Cd-3. The oxygen % includes the % of the rest of elements detected by EDS (TEM) and not shown in the Table. The last column showsn the pH values of the final mixture corresponding to the different cadmium (II) incorporation reactions.

	O (%)	Na (%)	P (%)	Ti (%)	Hg (%)	pH
TPNP	65,55 (± 4,80)	3,68 (± 0,13)	22,18 (± 3,33)	8,59 (± 1,37)	0,00	
TPNP-Hg-1	70,67 (± 2,22)	0,67 (± 0,08)	19,07 (± 1,24)	8,57 (± 0,63)	**1,03 (± 0,42)**	1,98
TPNP-Hg-2	70,00 (± 2,33)	1,29 (± 0,19)	18,67 (± 1,51)	7,90 (± 0,70)	**2,14 (± 0,20)**	3,74

Table 2. Relative concentration of O, Na, P, Ti and Cd (EDS (TEM) data) in TPNP, TPNP-Hg-1 and TPNP-Hg-2. The oxygen % includes the % of the rest of elements detected by EDS (TEM) and not shown in the Table. The last column shows the pH values of the final mixture corresponding to the different mercury (II) incorporation reactions.

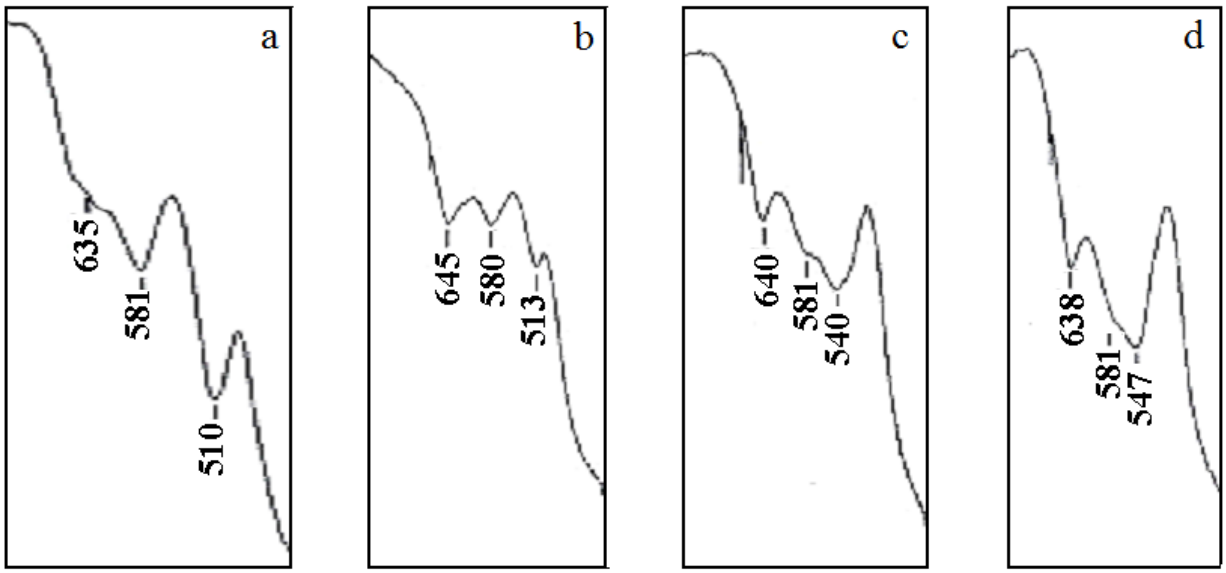

Figure 1. Infrared spectra in the region 700-400 cm^{-1} of TPNP (a), TPNP-Cd-1(b), TPNP-Cd-2 (c) and TPNP-Cd-3 (d).

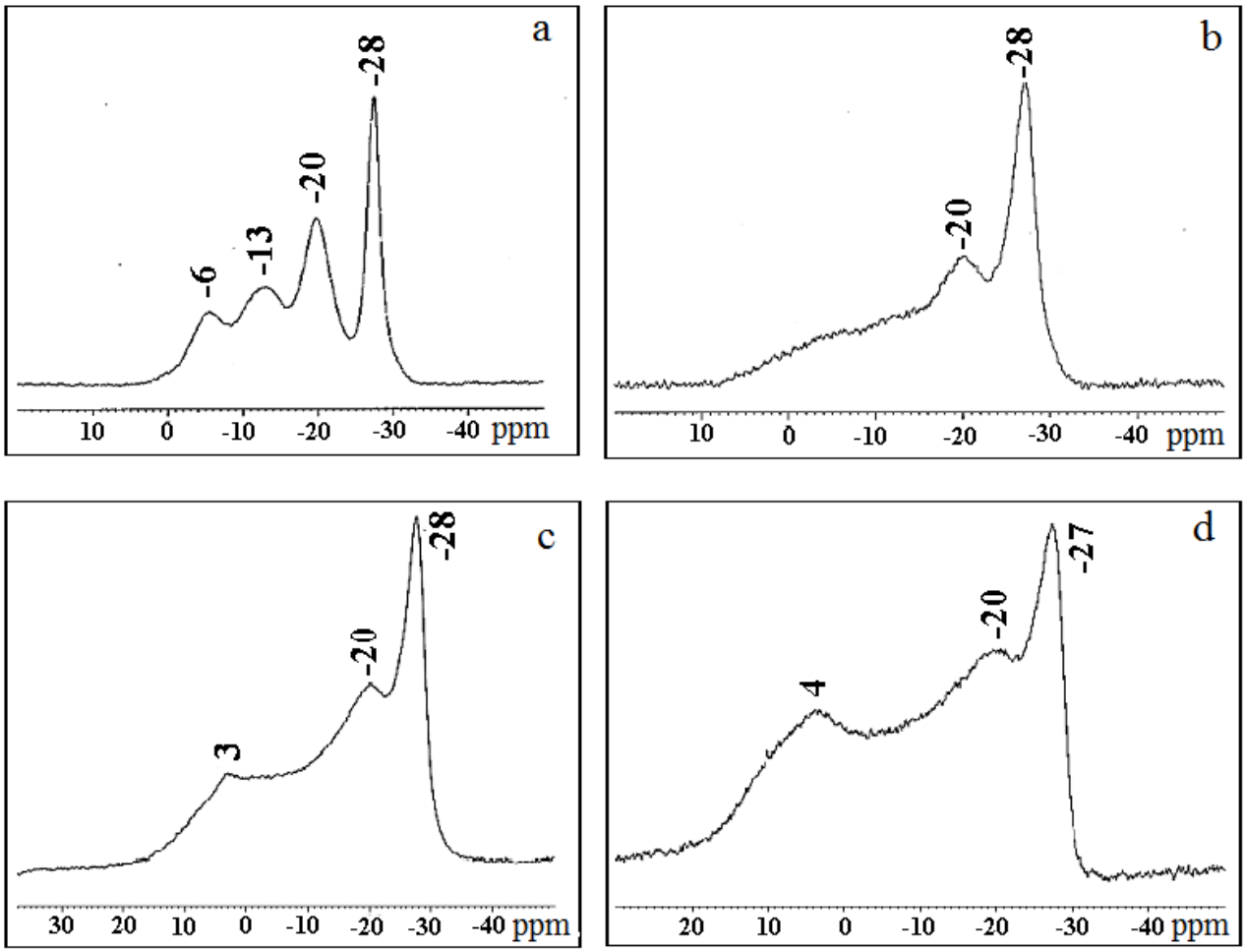

581

582 **Figure 2.** ^{31}P MAS NMR spectra of TPNP (a), TPNP-Cd-1(b), TPNP-Cd-2 (c) and TPNP-Cd-3 (d).

583

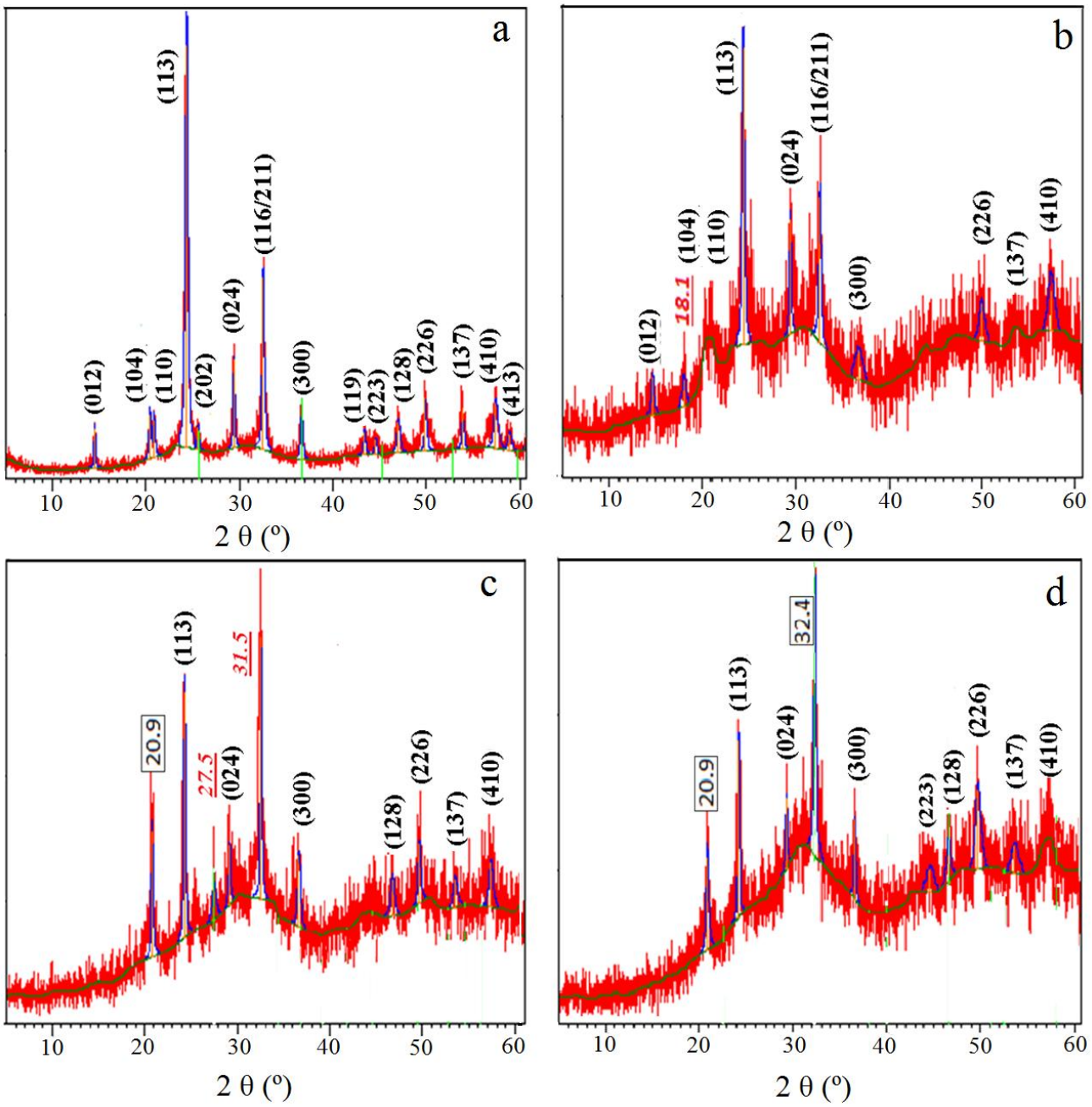

584

585 **Figure 3.** XRD patterns of TPNP (a), TPNP-Cd-1(b), TPNP-Cd-2 (c) and TPNP-Cd-3(d).

586

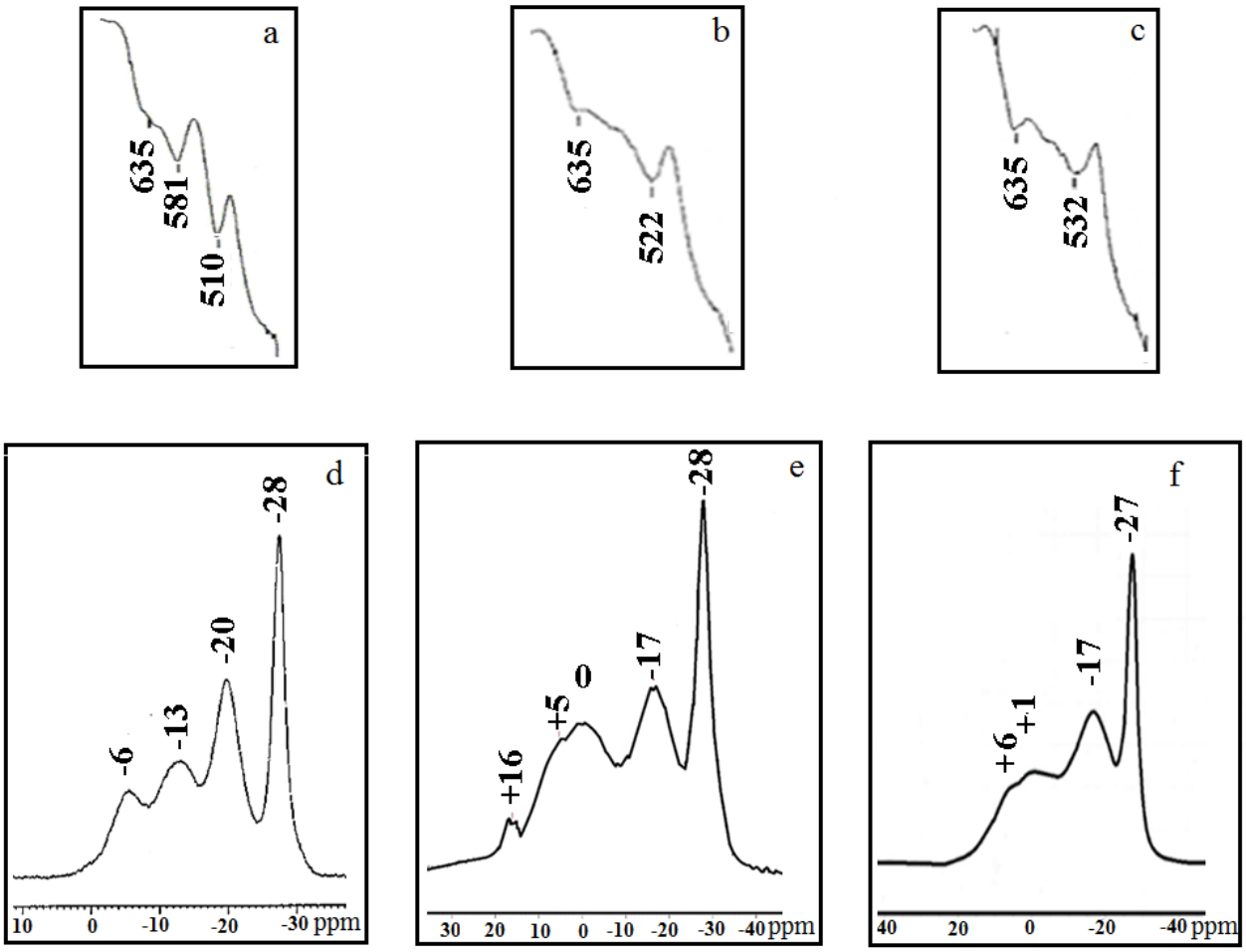

587

588 **Figure 4.** Infrared spectra in the region 700-400 cm^{-1} of TPNP (a), TPNP-Hg-1(b) and TPNP-Hg-2

589 (c) (top) and ^{31}P MAS NMR spectra of TPNP (d), TPNP-Hg-1(e) and TPNP-Hg-2 (f) (bottom).

590

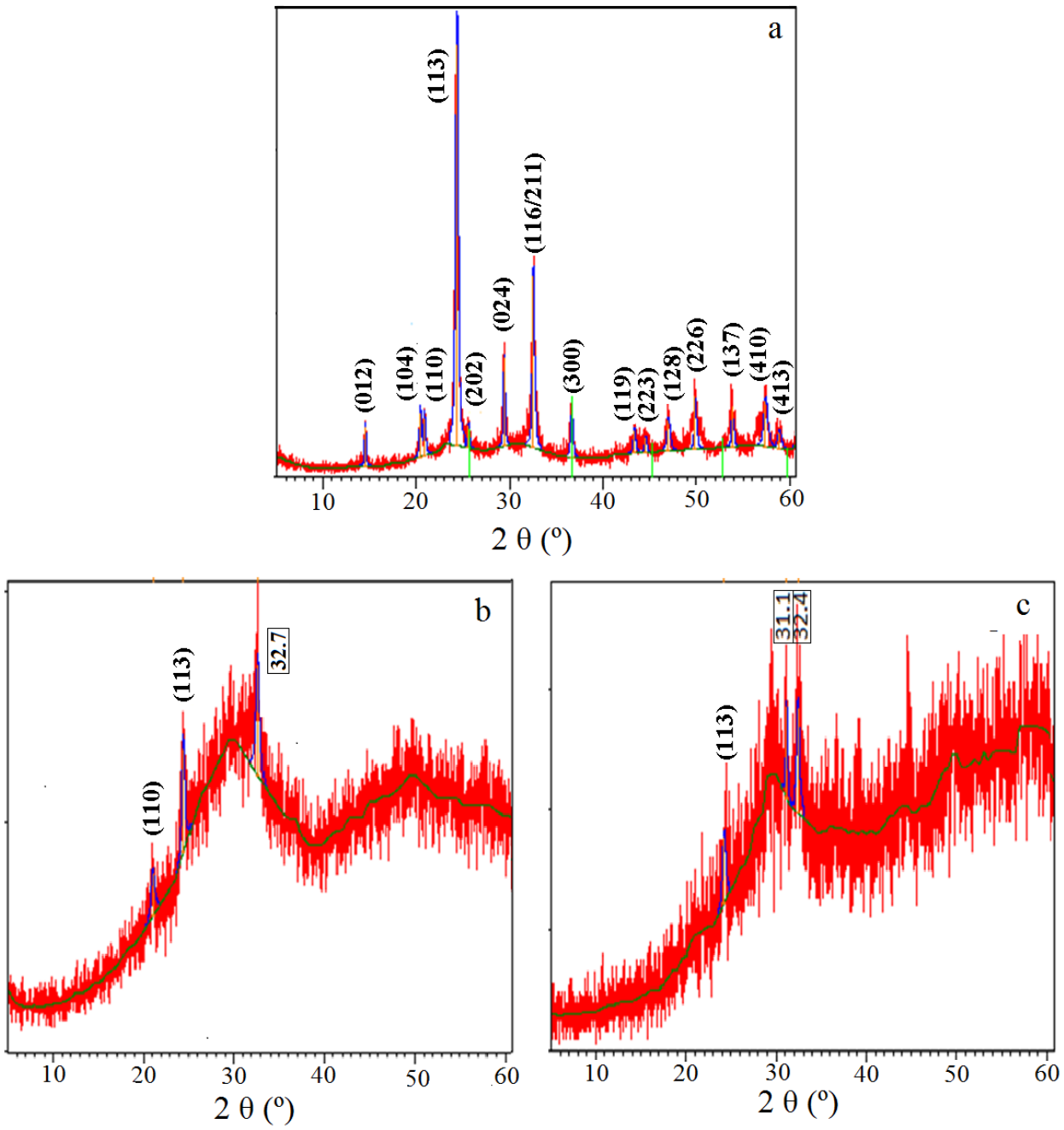

591

592 **Figure 5.** XRD patterns of TPNP(a), TPNP-Hg-1 (b) and TPNP-Hg-2 (c).

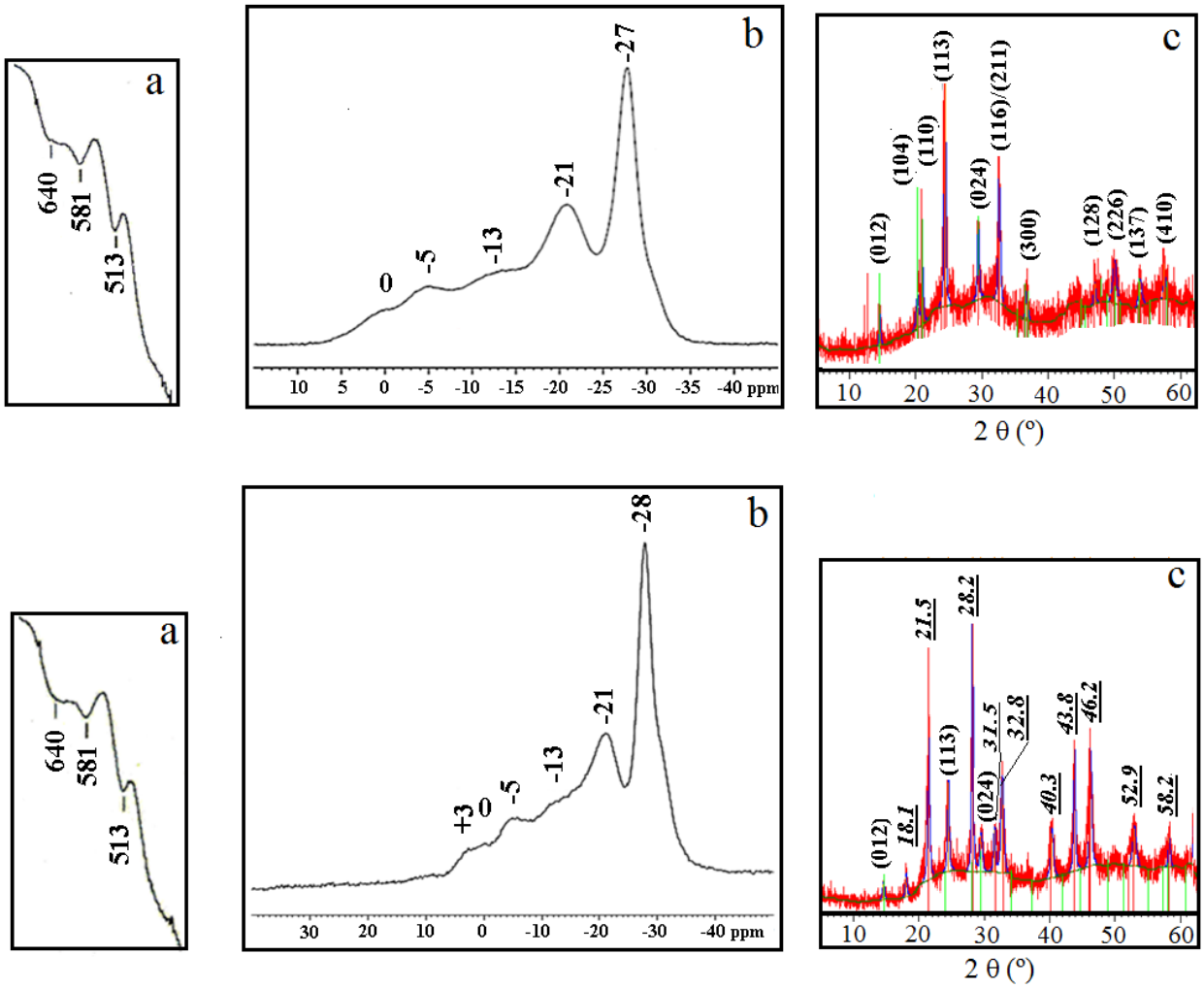

593

594 **Figure 6.** Infrared spectra in the region 700-400 cm^{-1} (a) ^{31}P MAS NMR spectra (b) and XRD

595 patterns (c) of TPNP-Cd-2-H (top) and TPNP-Hg-2-H (bottom).

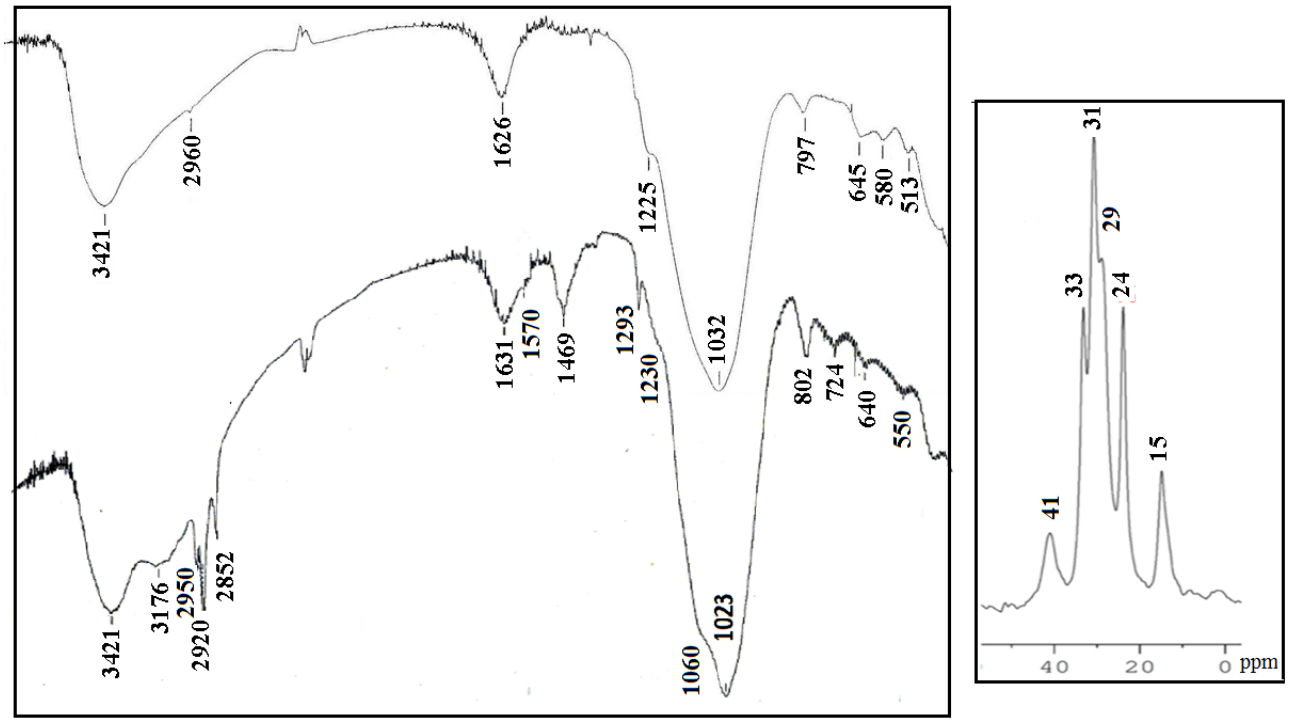

596

597 **Figure 7.** Infrared spectra (left) of TPNP-Cd-1 (top) and TPNP-Cd-1-OA (bottom) and ^{13}C CP/MAS

598 NMR spectra of TPNP-Cd-1-OA (right).

599

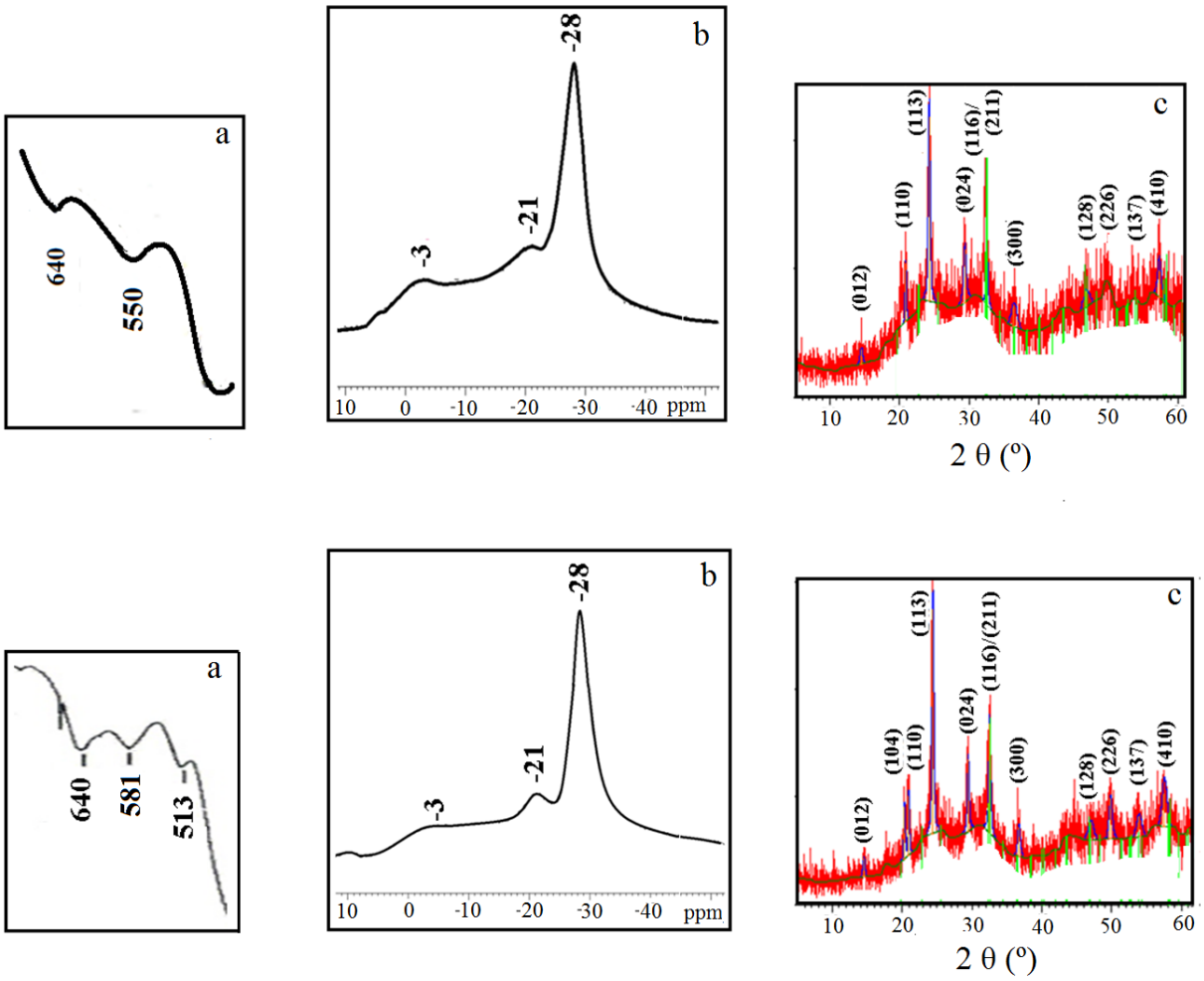

Figure 8. Infrared spectra in the region 700-400 cm^{-1} (a) ^{31}P MAS NMR spectra (b) and XRD patterns (c) of TPNP-Cd-1-OA (top) and TPNP-Cd-1-OA-H (bottom).

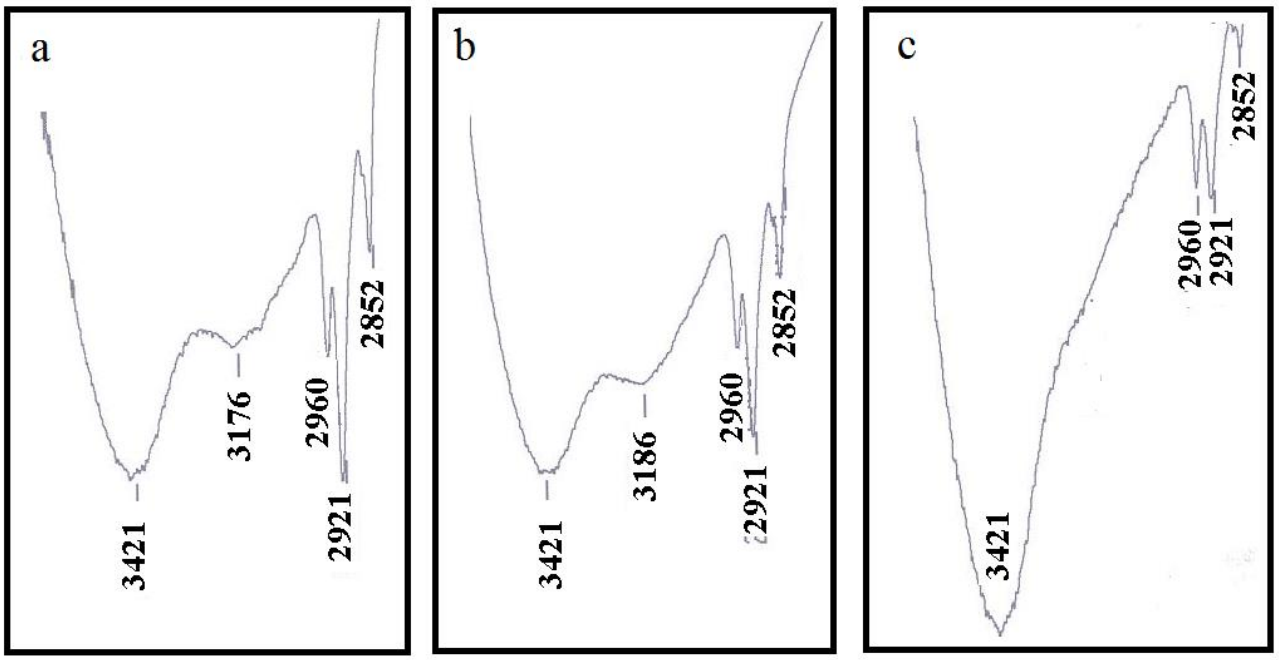

603

604 **Figure 9.** Infrared spectra in the region 4000-2800 cm^{-1} of TPNP-Cd-1-OA (a), TPNP-Cd-2-OA (b)

605 and TPNP-Cd-3-OA (c).

606

607

608

SUPPORTING INFORMATION

Sequential incorporation of metallic cations (Cd^{2+} and Hg^{2+}) and N-Octylamine into Titanium Phosphate Nanoparticles and their subsequent release in acid media

Javier Carrasco-Rodríguez[a], *Daniel Martín-Yerga*[b], *Leoncio Garrido*[c], *Agustín Costa-García*[b], *Francisco J. García Alonso**[a].

a) Nanobioanalysis group, Department of Inorganic and Organic Chemistry, University of Oviedo, 33006, Oviedo (Spain)

b) Nanobioanalysis Group, Department of Physical and Analytical Chemistry, University of Oviedo, 33006, Oviedo (Spain)

c) Departamento de Química Física, Instituto de Ciencia y Tecnología de Polímeros, ICTP-CSIC, Juan de la Cierva 3, 28006 Madrid, Spain

* Corresponding author: Francisco J. García Alonso, fjga@uniovi.es

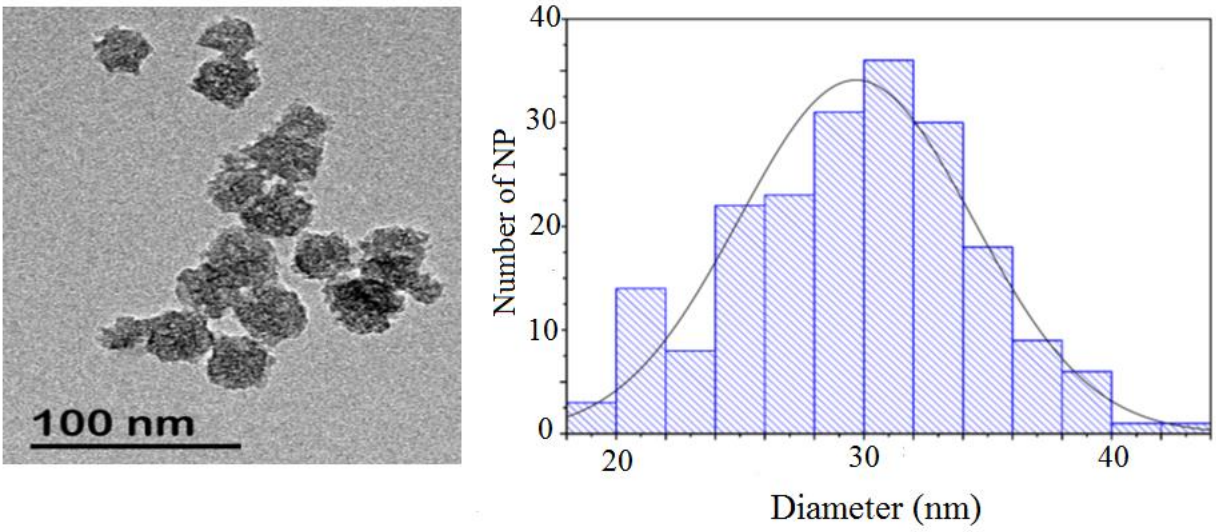

Figure S-1 TEM Micrographs (left) and Size distribution (right) of TPNP.

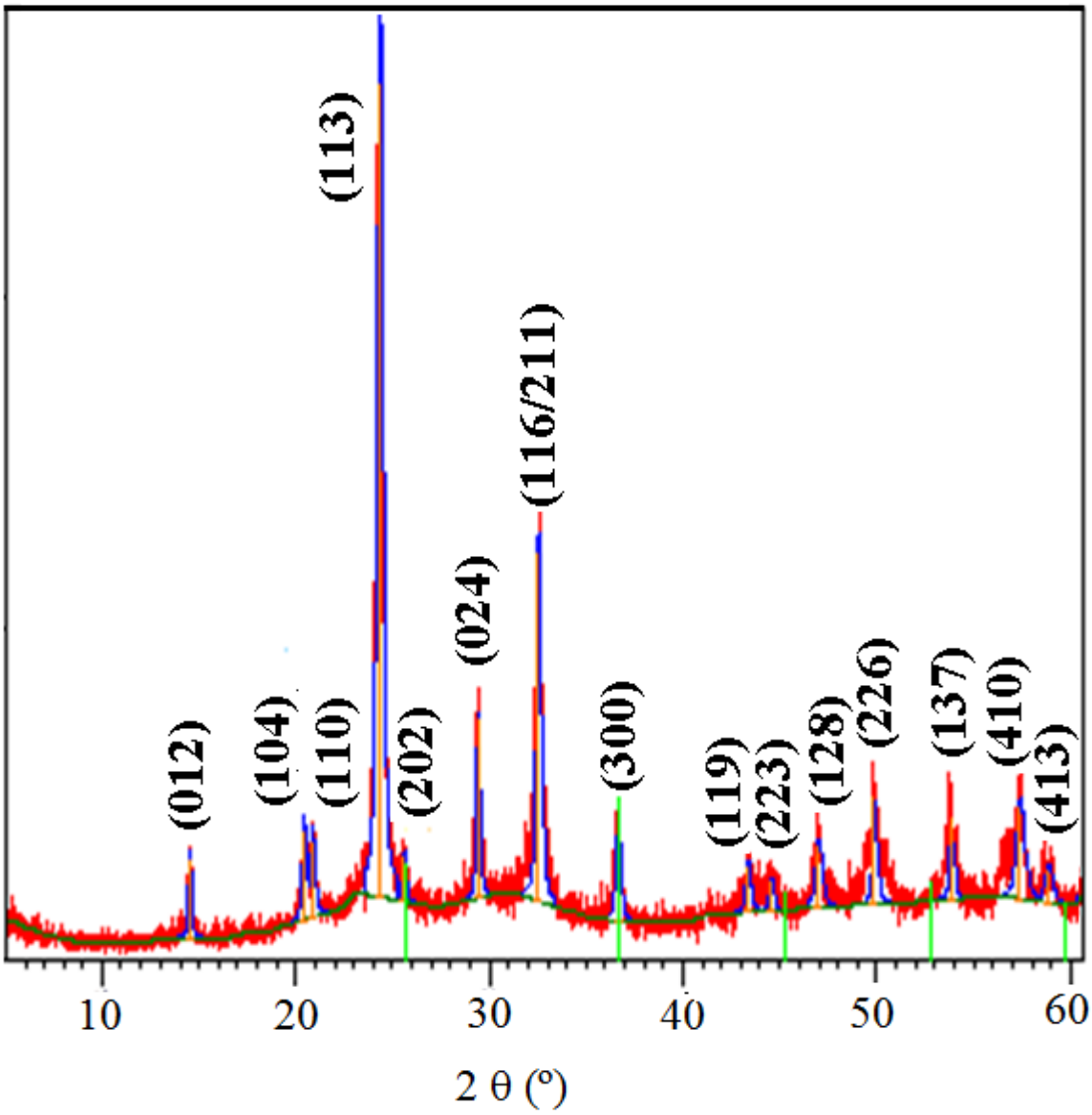

Figure S-2 XRD pattern of TPNP.

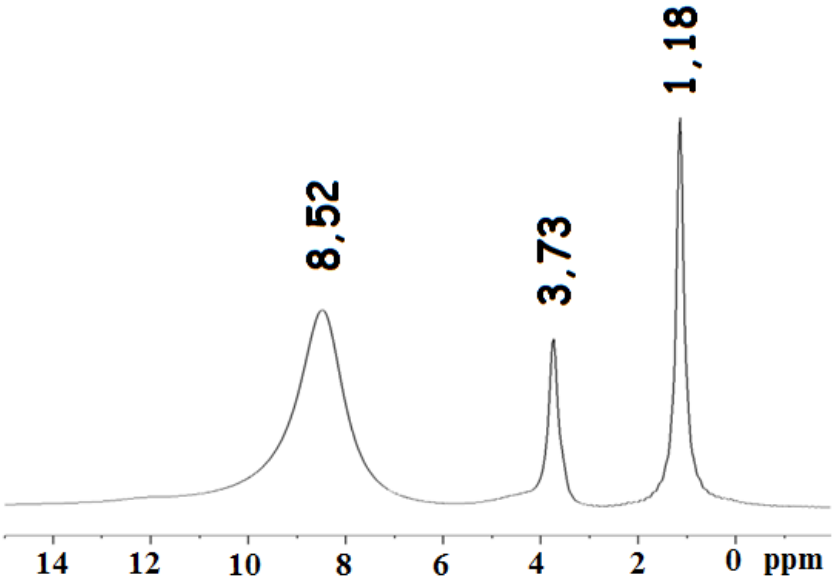

Figure S-3 ^{1}H MAS NMR of TPNP.

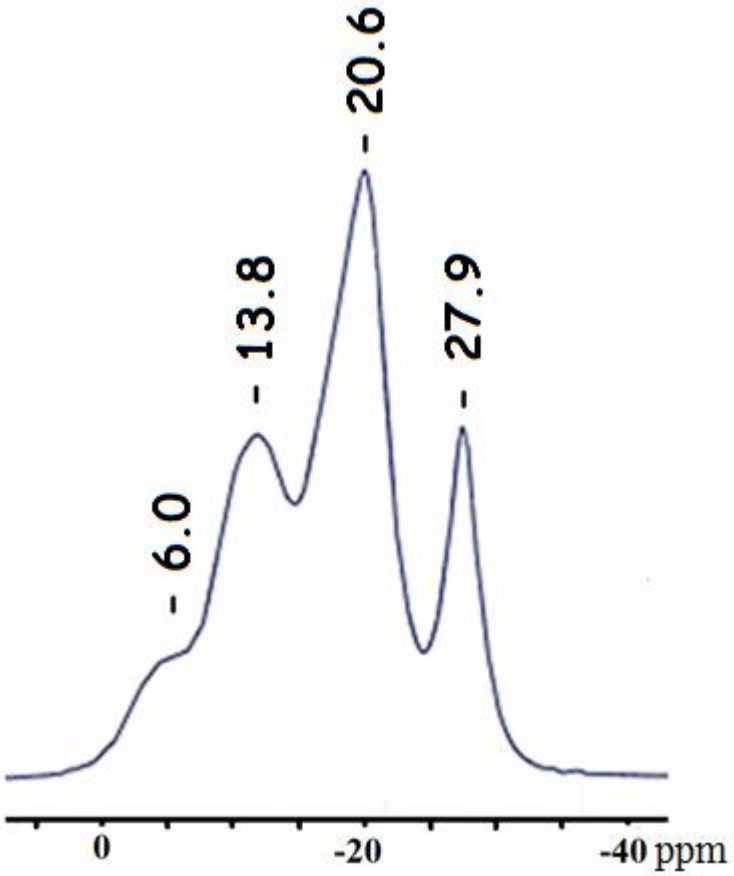

Figure S-4 ^{31}P CP/MAS NMR spectrum of TPNP.

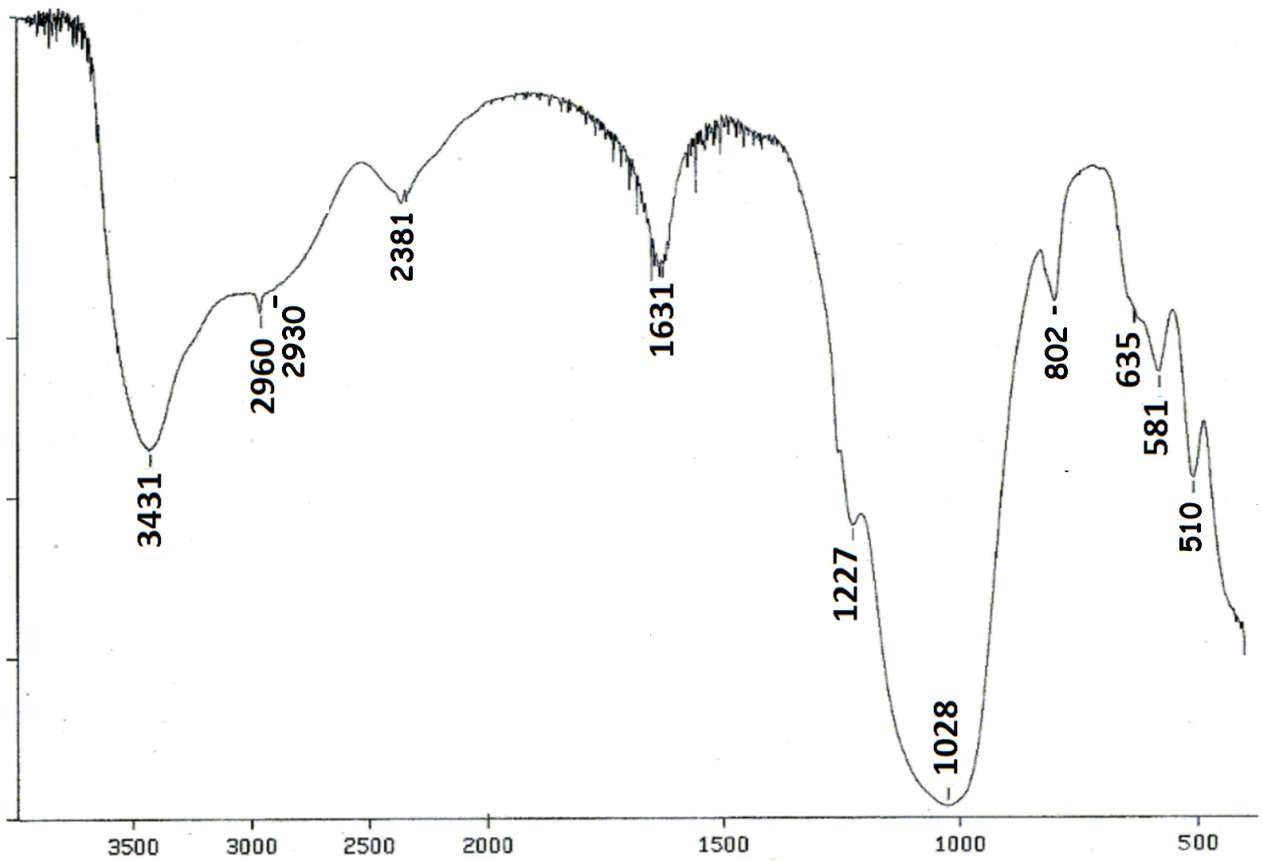

Figure S-5 Infrared spectrum of TPNP (4000-400 cm^{-1}).

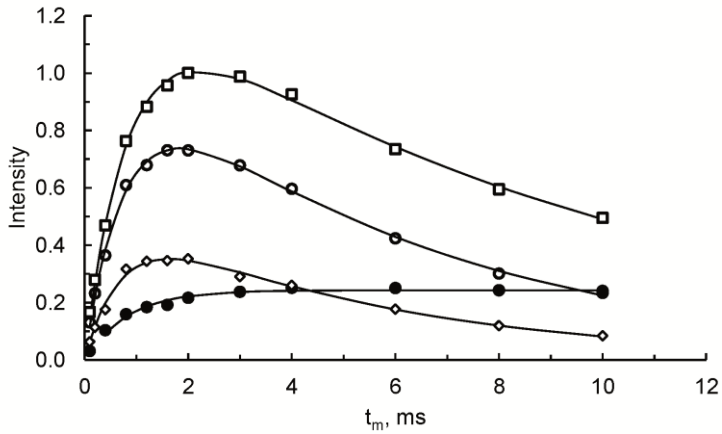

Figure S-6. $^{1}H \rightarrow {}^{31}P$ CP kinetics with MAS at 6 kHz in TPNP: (●) -27.9 ppm; (□) -20.6 ppm; (○) -13.8 ppm, and (◊) -6.0 ppm. The fittings use eq. $I(t) = I_0\,(1 - \frac{T_{IS}}{T_{1\rho}^{I}})^{-1}\left[\exp\left(-\frac{t_m}{T_{1\rho}^{I}}\right) - \exp(-\frac{t_m}{T_{IS}})\right]$ where *I(t)* represents the peak intensity, I_0 is the absolute intensity, T_{IS} is the CP time constant between nuclei *I* (^{1}H) and *S* (^{31}P), $T_{1\rho}^{I}$ is the spin-lattice relaxation time in the rotating frame of nuclei *I* and t_m is the contact time.

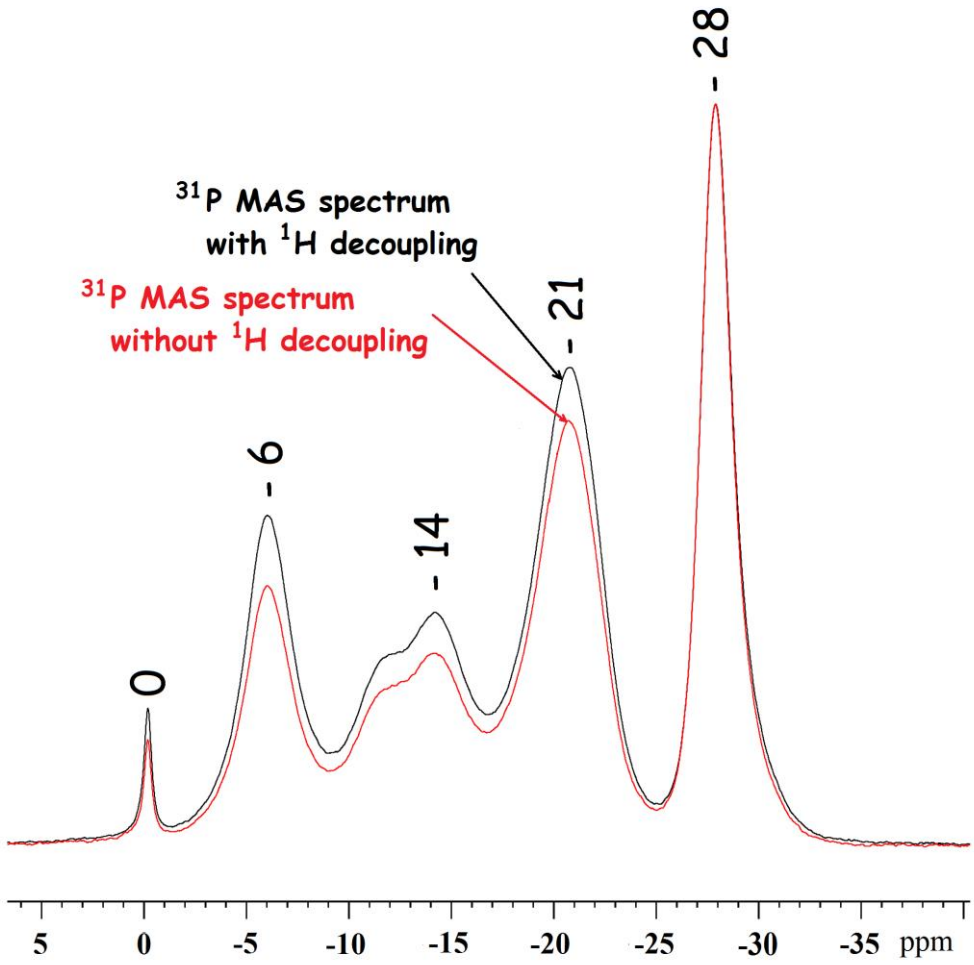

Figure S-7 ^{31}P MAS NMR spectra of TPNP, one with ^{1}H decoupling (black), the other without ^{1}H decoupling (red).

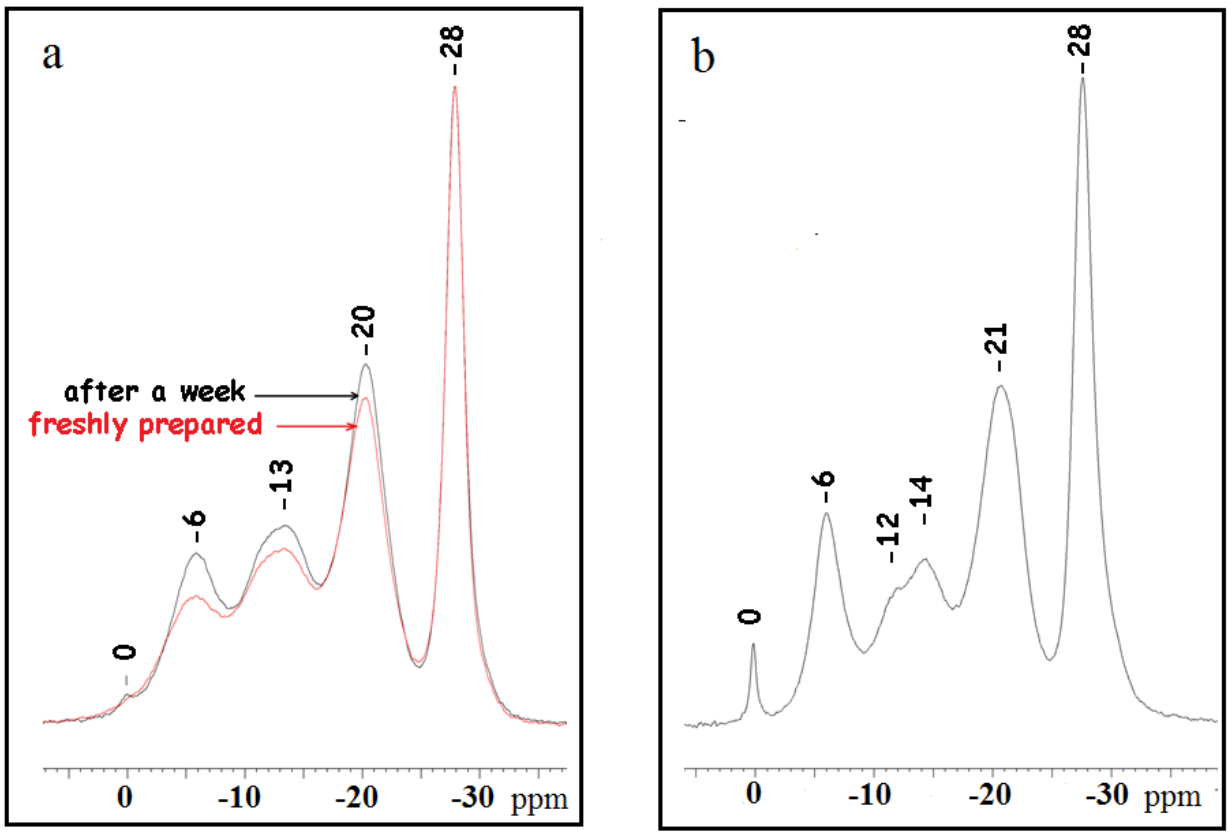

Figure S-8 ^{31}P MAS NMR spectrum of TPNP freshly prepared (red) and after a week (black) (a) and after four months (b).

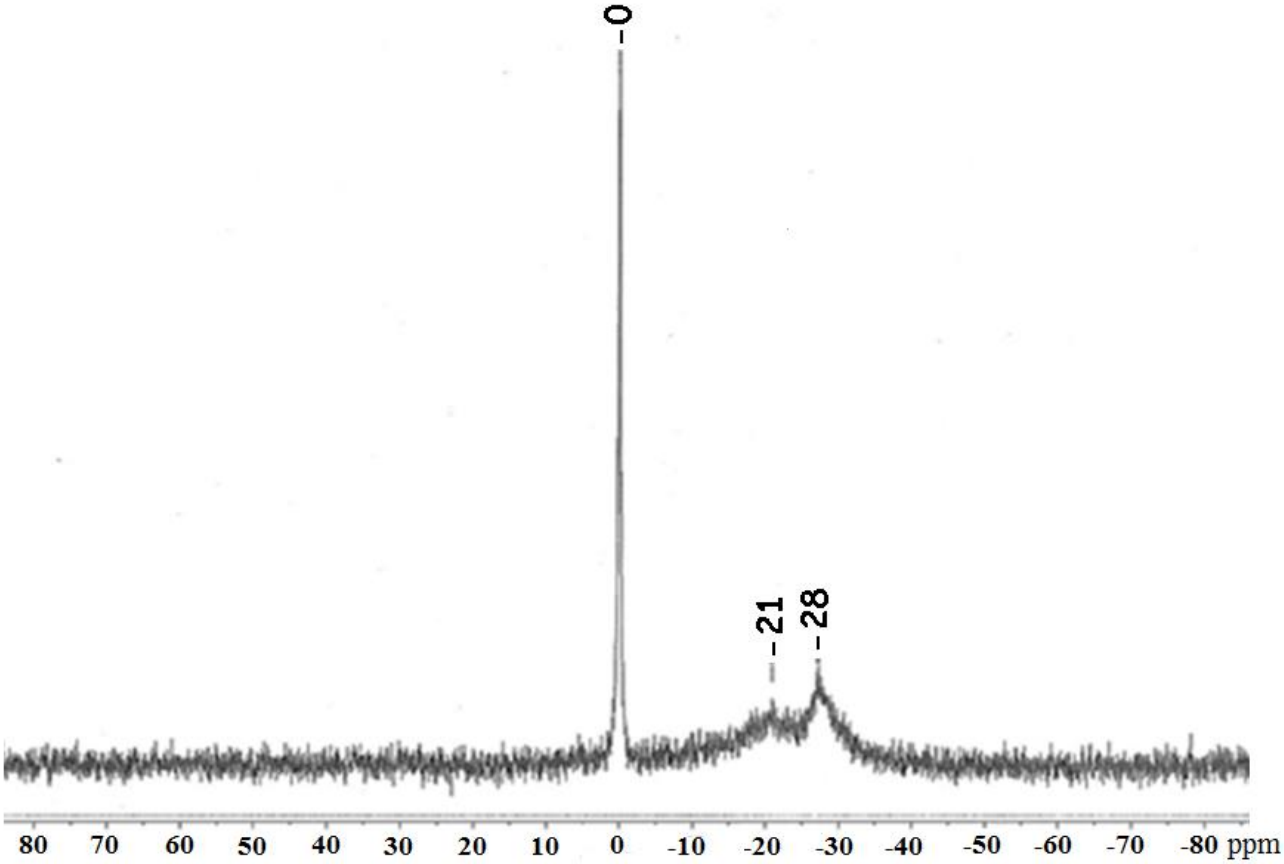

Figure S-9 ^{31}P NMR spectrum of TPNP in D_2O after stirring at room temperature the nanoparticles in deuterated water for 10 minutes.

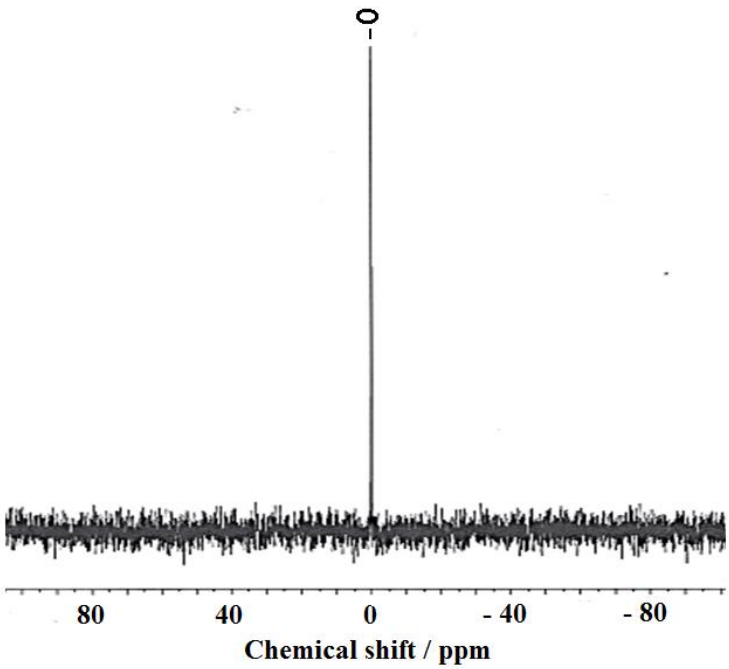

Figure S-10 ^{31}P NMR spectrum of the final mixture solution after the reaction between TPNP (40 mg) and $Cd(NO_3)_2$ (0.17 mmol) at 50ºC for 2h. Initially, the titanium phosphate nanoparticles were added to the cadmium salt solution.

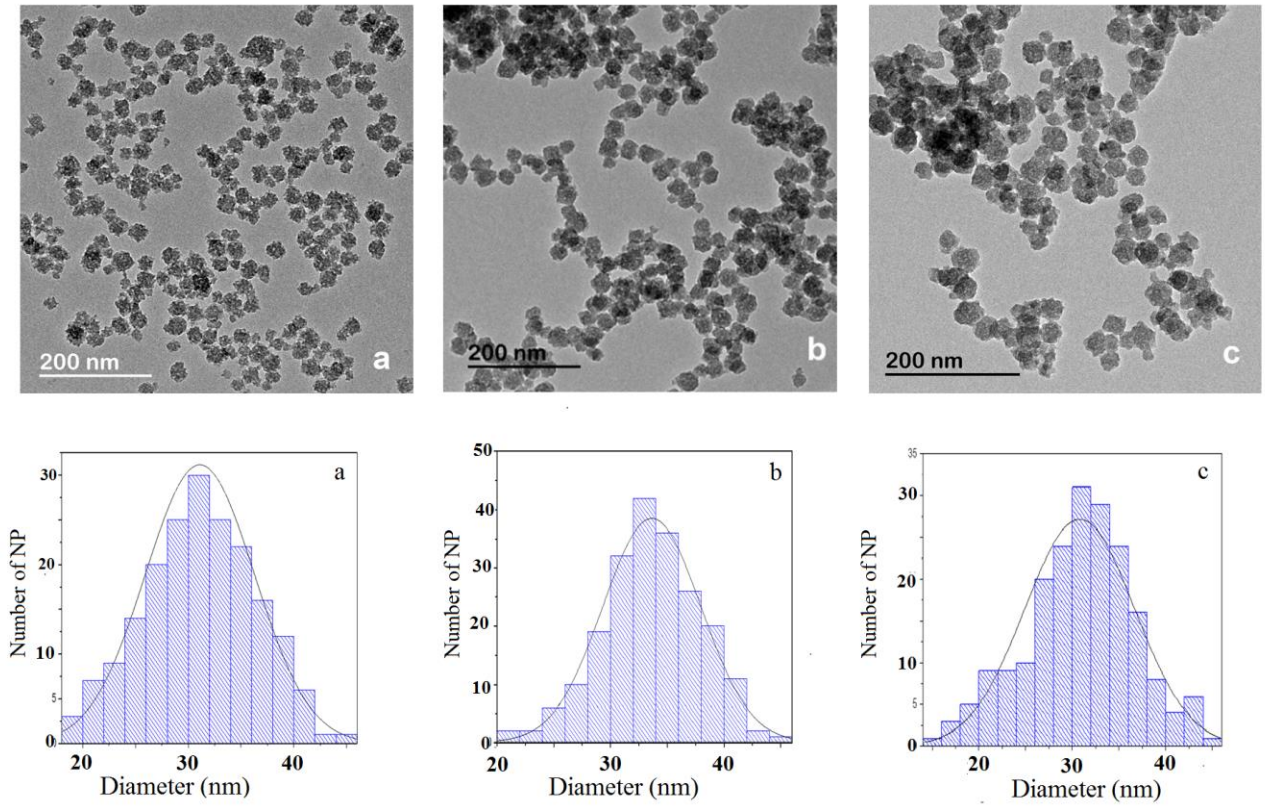

Figure S-11 TEM Micrographs (top) and Size distribution (bottom) of TPNP-Cd-1(a), TPNP-Cd-2 (b) and TPNP-Cd-3 (c).

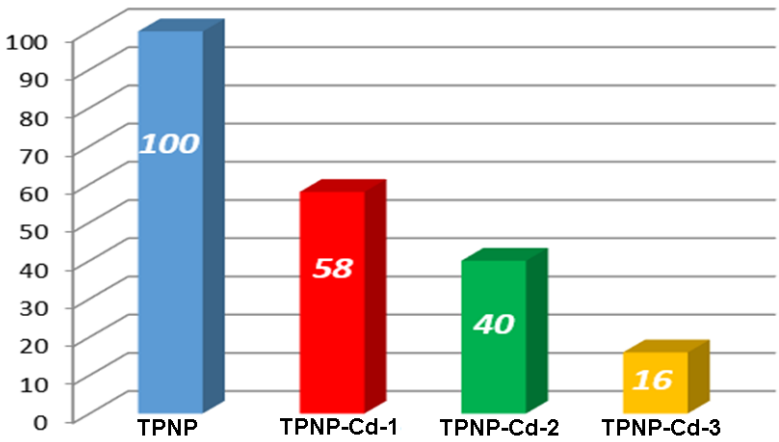

Figure S-12 Relative area under the fluorescence signal at 720 nm corresponding to TPNP, TPNP-Cd-1, TPNP-Cd-2 and TPNP-Cd-3.

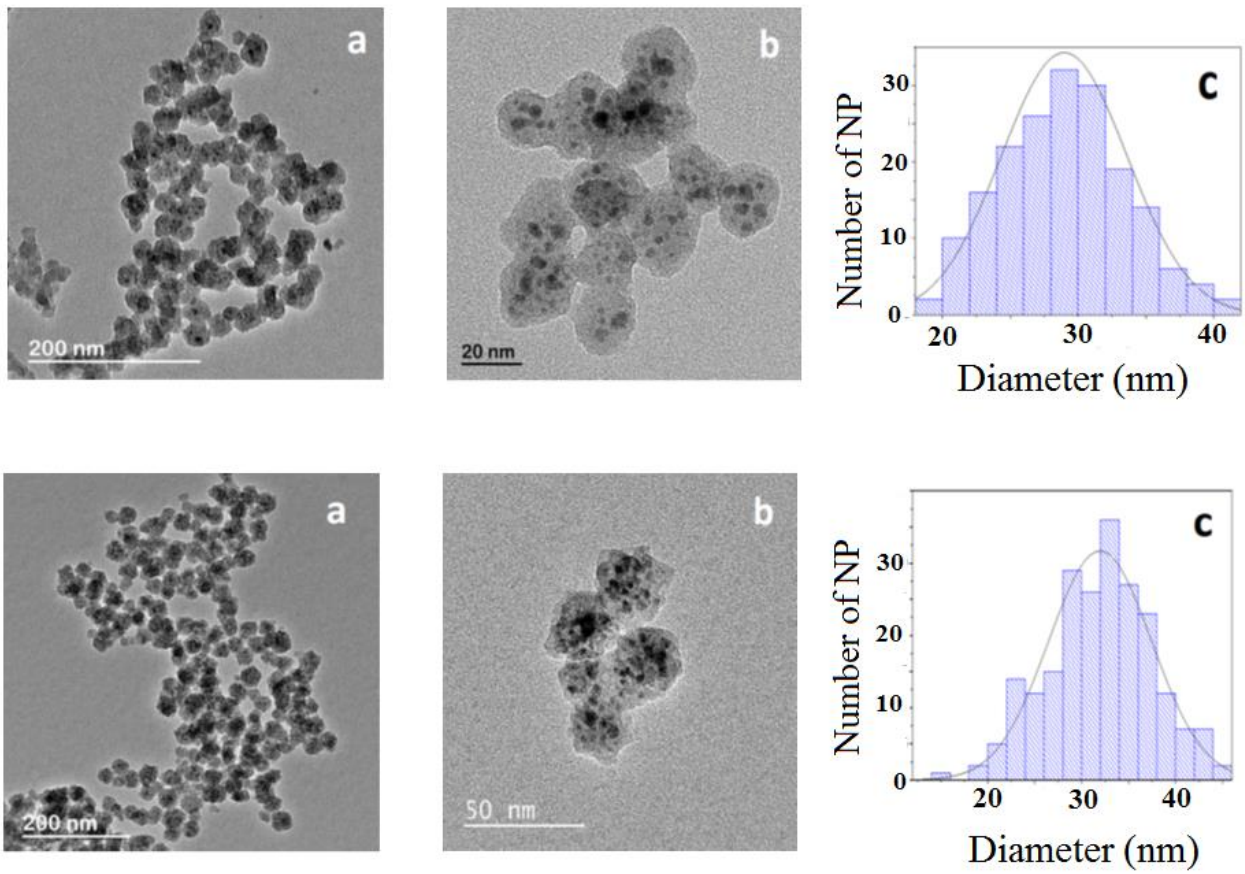

Figure S-13 Overview (a) and detailed (b) TEM Micrographs and Size distribution (c) of TPNP-Hg-1 (top) and TPNP-Hg-2 (bottom).

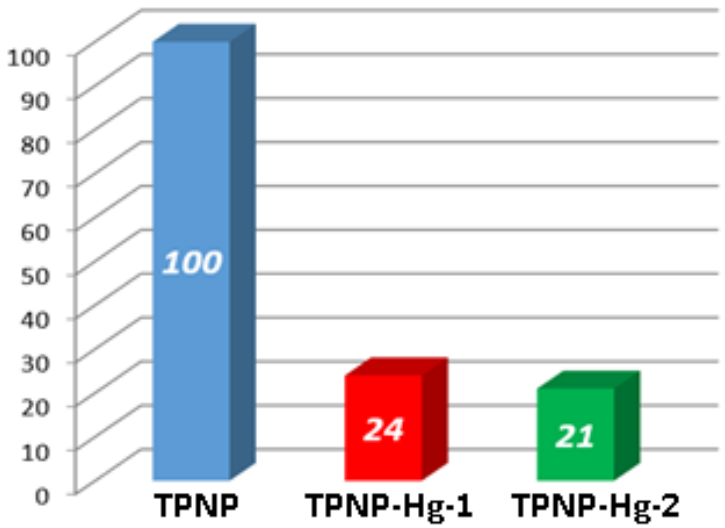

Figure S-14 Relative area under the fluorescence signal at 720 nm corresponding to TPNP, TPNP-Hg-1 and TPNP-Hg-2.

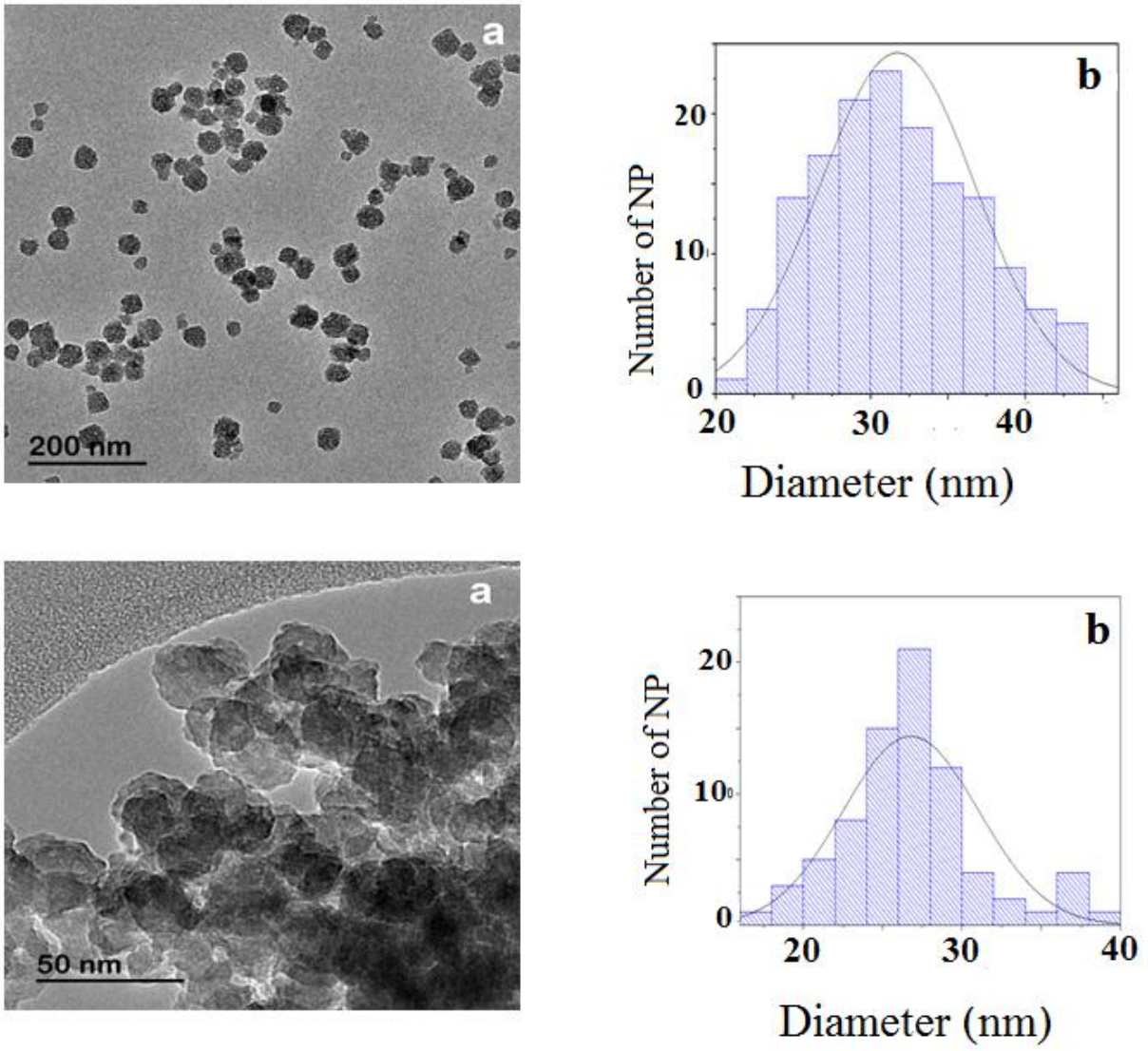

Figure S-15 TEM Micrographs (a) Size distribution (b) of TPNP-Cd-2-H (top) and TPNP-Hg-2-H (bottom).

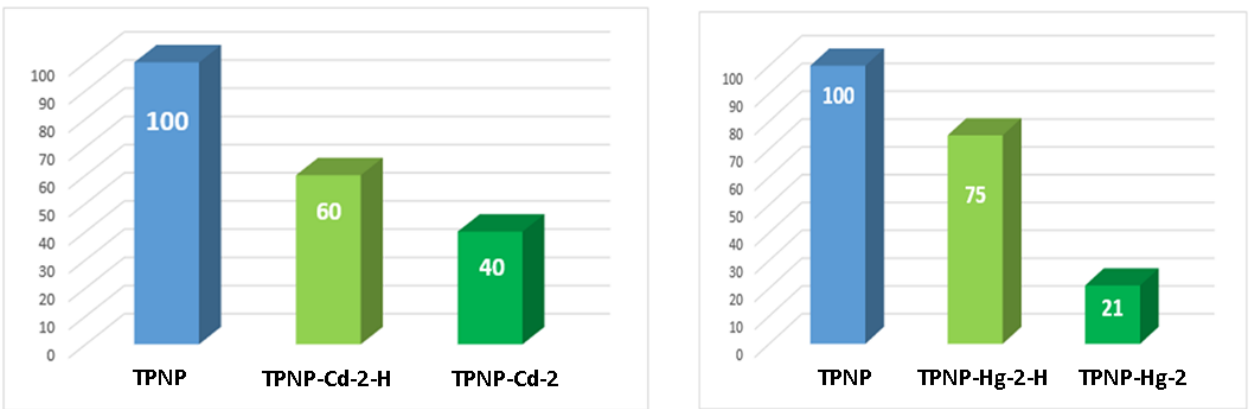

Figure S-16 Relative area under the fluorescence signal at 720 nm corresponding to TPNP, TPNP-Cd-2-H and TPNP-Cd-2 (left) and to TPNP, TPNP-Hg-2-H and TPNP-Hg-2 (right).

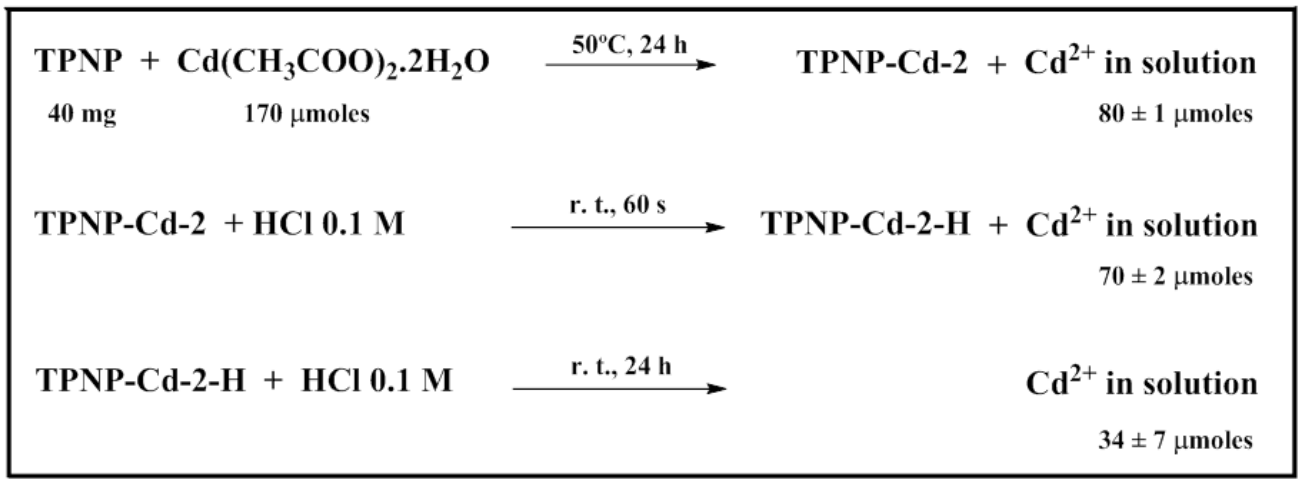

Figure S-17 Monitoring of Cd^{2+} abundance in solution and the incorporation /release of the cadmium (II) cation to/from titanium phosphate nanoparticles.

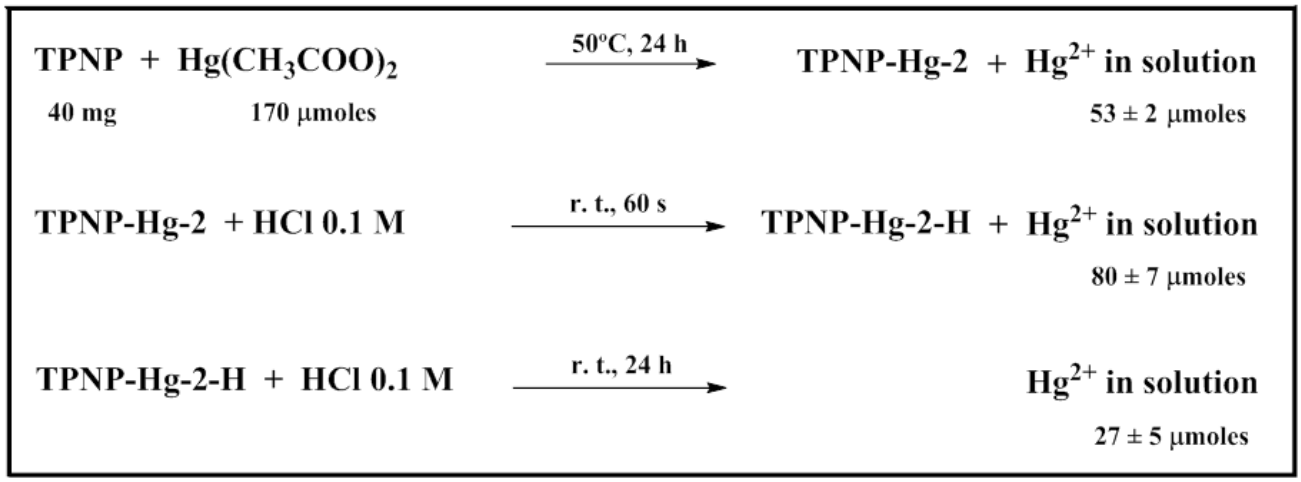

Figure S-18 Monitoring of Hg^{2+} abundance in solution and the incorporation/release of the mercury (II) cation to/from titanium phosphate nanoparticles.

Table S-1. Cross-polarization time constants.

Phosphate group	δ_{iso}, ppm	$T_{1\rho}$ (^{1}H) [a], ms	T_{HP}[a], ms
$(PO_4)^{3-}$	-27.9	∞	0.83 (0.06)
$(HPO_4)^{2-}$	-20.6	9.6 (0.4)	0.83 (0.03)
$(H_2PO^4)^-$	-13.8	6.2 (0.2)	0.78 (0.03)
(NaH_2PO_4)	-6.0	5.2 (0.4)	0.71 (0.06)

[a]Standard deviation shown in parenthesis.